

WORTECS



**H2020-ICT-2016-2
RIA**



**Project-ID: 761329
WORTECS**

Networking research beyond 5G

D3.2

Common Analog and Digital Baseband Design for Flexible Radio and Optical Transceiver

Contractual Date of Delivery:	2018, November 30th
Actual Date of Delivery:	
Editor(s):	Guillaume Vercasson (BCM)
Author(s):	Guillaume Vercasson, Rodolphe Legouable, Jean Dion (BCM), Tiwari Krishan Kumar, Brzozowski Marcin, Sark Vladica (IHP), Camilo Valencia, Jorge Garcia, Huetzin Perez (Oledcomm), Olivier Bouchet (Orange), Mir Ghoraihi (pureLiFi), Ravinder Singh, Dominic O'Brien, Grahame Faulkner (UOXF), Rafael Pérez, Víctor Guerra, José Rabadan (UNIVERSIDAD DE LAS PALMAS)
Work package:	WP3
Security:	PU
Nature:	Deliverable
Version:	version 1.4
Total number of pages:	36

Abstract

This deliverable focuses especially on radio and optical transmissions. The main issue of this document is to try to find a common architecture between the radio and optical transmitter in order to mutualize as much as possible the implementation.

Starting from the analysis of the propagation channel characteristics of both systems, we argue about the choice of the modulation format when also taking into account some material constraints issued from the hardware components. Then, Tx and Rx description and limitations of analog radio and optical parts are pointed out before describing the main elements composing the radio and optical baseband system physical layer. In conclusion, we propose three main possibilities for mutualizing the radio and optical transmitter platforms.

Keyword list

Optical wireless transmission, radio transmission, mutualisation, reconfigurable, OFDM, Single Carrier, Channel modelling, RF, baseband, HW implementation



List of Authors

First name	Last name	Beneficiary	Email address
Guillaume	Vercasson	b<>com	guillaume.vercasson@b-com.com
Rodolphe	Legouable	b<>com	Rodolphe.legouable@b-com.com
Krishan Kumar	Tiwari	IHP	tiwari@ihp-microelectronics.com
Mohamed Hussein	Eissa	IHP	eissa@ihp-microelectronics.com
Mohammed	Ramadan	IHP	ramadan@ihp-microelectronics.com
Marcin	Brzozowski	IHP	brzozowski@ihp-microelectronics.com
Vladica	Sark	IHP	sark@ihp-microelectronics.com
Mir	Ghoraishi	pureLiFi	mir.ghoraishi@purelifi.com
Jorge	García-Márquez	OLD	jorge.garcia@oledcomm.com
Olivier	Bouchet	ORANGE	olivier.bouchet@orange.com
Ravinder	Singh	UOXF	ravinder.singh@eng.ox.ac.uk
Dominic	O'Brien	UOXF	dominic.obrien@eng.ox.ac.uk
Rafael	Pérez Jiménez	ULPGC	rperez@dsc.ulpgc.es
Víctor	Guerra Yáñez	ULPGC	victor.guerra@fpct.ulpgc.es

Document History

First name	Last name	Version	Comments
Guillaume	Vercasson	2018 - Nov 22 th	First draft
Krishan Kumar	Tiwari	2018 – Nov 28 th	First IHP contribution
Victor	Guerra	2018 – Dec 17 th	ULPGC channel propagation contribution
Vladica	Sark	2018 – Dec 18 th	Update of IHP contribution
Mir	Ghoraishi	2018 – Dec 23 rd	PureLiFi optic contribution
Rodolphe	Legouable	2019 – Jan 10 th	b<>com contribution and working document
Guillaume	Vercasson	2019 – Jan 11 th	b<>com contribution and working document
Jorge	Garcia	2019 – Jan 11 th	OLD contribution on Analog OWC front-end
Guillaume	Vercasson	2019 – Jan 14 th	b<>com : document merging and formatting
Victor	Guerra	2019 – Jan 15 th	Answer to OWC channel propagation section
Mir	Ghoraishi	2019 – Jan 17th	Inputs to section 5.2 and document review
Jorge	Garcia	2019 – Jan 11 th	OLD contribution on Analog OWC front-end
Guillaume	Vercasson	2019 – Jan 21 th	BCM contribution on mutualisation exemple
Vladica	Sark	2019 – Jan 22 th	IHP contribution on digital base band module
Guillaume & Rodolphe	Vercasson & Legouable	2019 – Jan 22th	Merging and revised document
Victor	Guerra	2019 – Jan 23 th	Global review
Mir	Ghoraishi	2019 – Jan 23th	Global review
Guillaume	Vercasson	2019 – Jan 24 th	Global review and correction of section 6
Jorge	Garcia	2019 – Jan 24 th	Global review and reply to some comments
Vladica	Sark	2019 – Jan 29 th	IHP general review and addings

List of Acronyms

Acronym	Meaning
ACO-OFDM	Asymmetrically Clipped Optical OFDM
ADC	Analog to Digital Converter
A/D	Analog to Digital
AFE	Analog Front End
APD	Avalanche Photodiode
ASIC	Application-Specific Integrated Circuit
AWG	Additive White Gaussian
AWGN	Additive White Gaussian Noise
BER	Bit Error Rate
BP	Believe Propagation
CP	Cyclic Prefix
CIR	Channel Impulse Response
CFO	Carrier Frequency Offset
dB	Decibel
D/A	Digital to Analog
DAC	Digital-to-Analog Converter
DC	Direct Current
DCO-OFDM	DC biased Optical OFDM
DFT	Discrete Fourier Transform
DVB	Digital Video Broadcasting
EIRP	Effective Isotropic Radiated Power
FEC	Forward Error Code
FFC	Free-From Optical Concentrator
FFT	Fast Fourier Transform
FIR	Finite Impulse Response
FBMC	Filter-Bank Multicarrier
FOV	Field of View
FPGA	Field Programmable Gate Array
FWHM	Full Width at Half Maximum
Gbps	Giga bits per second
GND	Ground
HMD	Head Mounted Display
HSPA	High Speed Packet Access
IFFT	Inverse Fast Fourier Transform
IM/DD	Intensity Modulation / Direct Detection
IR	Infra-Red
ISI	Inter Symbol Interference
LDPC	Low Density Parity Check
LED	Light-Emitting Diode
LO	Local Oscillator
LOS	Line Of Sight
LTE	Long Term Evolution
MAC	Medium Access Control
MCRT	Monte Carlo Ray Tracing
MCS	Modulation and Coding Scheme

MIMO	Multiple-Input Multiple-Output
NIR	Near Infra-Red
NLOS	Non Line Of Sight
OFDM	Orthogonal Frequency Division Multiplex
OFDM-MConst	OFDM with multiple constellations
OFE	Optical Front End
OOB	Out Of the Band
O-OFDM	Optical OFDM
ODH	Optical Detector Head
OTH	Optical Transmission Head
OWC	Optical Wireless Communication
PA	Power Amplifier
PAM- DMT	Pulse-Amplitude-Modulated Discrete-Multitone
PAPR	Peak-to-Average Power Ratio
PCB	Printed Circuit Board
PCC	Parabolic Compound Concentrator
PHy	Physical layer
PRBS	Pseudo-Random Binary Sequence
P/S	Parallel to Serial
QC-LDPC	Quasi-Cyclic LDPC
RF	Radio Frequency
RMS	Root Mean Square
SC	Single Carrier or Successive-Cancellation
SCL	Successive-Cancellation List
SISO	Single Input Single Output
SNR	Signal to Noise Ratio
S/P	Serial to Parallel
SP	Sum-Product
SPI	Serial Peripheral Interface
TIR	Total Internal Reflections
UFMC	Universal Filtered Multi-Carrier
VGA	Variable Gain Amplifier
VR	Virtual Reality
WORTECS	Wireless Optical/Radio TErabit CommunicationS
ZP	Zero Prefix

Table of contents

1	<i>Introduction</i>	8
2	<i>Propagation channel characteristics</i>	9
2.1	Optical channel	9
2.2	240 GHz radio channel	11
2.3	Radio and optical common channel parameters	12
3	<i>SC vs OFDM</i>	13
4	<i>Analog front-end</i>	14
4.1	Description & limitation both Tx and Rx radio front-end	14
4.1.1	Description of the Tx and Rx radio front-end.....	14
4.1.2	Limitation of the Tx and Rx radio front-end	15
4.2	Description and limitations of both Tx and Rx optical front-ends	15
4.2.1	First OWC Demonstrator	16
4.2.2	Block diagram of transmitter design	16
4.2.3	Second free form parabolic concentrator.....	17
4.2.4	Block diagram of AFE Receiver (Rx)	17
5	<i>Digital baseband</i>	18
5.1	Description of both Tx and Rx radio digital baseband	18
5.1.1	Channel bonding	18
5.1.2	Digital Baseband Architectures.....	19
5.1.3	Orthogonal Frequency Division Multiplexing (OFDM)	20
5.1.4	Forward Error Correction (FEC)	25
5.2	Description of digital baseband for OWC	27
5.2.1	Hermitian symmetry OFDM.....	27
5.2.2	Alternate approach: standard OFDM for OWC	28
6	<i>Common Radio and OWC architecture</i>	29
6.1	Strong mutualisation	29
6.2	Mutualisation example	29
6.3	Radio-optical common architecture	30
7	<i>Conclusion and perspectives</i>	31
8	<i>References</i>	33
9	<i>Appendix A</i>	35

List of Tables

Table 1 - Main optical Tx components	16
Table 2 - Optical Rx components	18
Table 3 - Summary for different waveforms, grades A to C indicate good to bad. [20]	20
Table 4 - Hardware efficiency of 3GPP LTE decoders.....	27
Table 5 - Mutualized OFDM system parameters example.....	29

List of Figures

Figure 1 - WORTECS Ray Tracing scheme.....	10
Figure 2 - Materials involved on the scenario.....	10
Figure 3 - Specific attenuation due to atmospheric gases, calculated at 1 GHz intervals, including line centers; ITU-R model.....	12
Figure 4 - Initial plan of the antenna array configuration.....	15
Figure 5 - WORTECS basic transmitter.....	16
Figure 6 - Tx OFE PCB.	16
Figure 7 - WORTECS second version of the free-form optical concentrator. At 30° it experiences a small entrance ray losses.....	17
Figure 8 - WORTECS Rx Optical Front End.	17
Figure 9 - Multiple neighbouring sub-channels exemple.....	18
Figure 10 - Block diagram of a paralelized OFDM transmitter	20
Figure 11 - OFDM based receiver data-path.....	23
Figure 12 - OFDM frame format	23
Figure 13 - Preamble format	23
Figure 14 - Delay and correlate algorithm for preamble detection	23
Figure 15 - FEC coding gain	25
Figure 13 - Hermitian smmetry OFDM Tx architecture	28
Figure 14 - Hermitian symmetry OFDM Rx architecture	28
Figure 15 - Proposed Tx architecture for OWC.....	29
Figure 16 - Propsoed Rx architecture for OWC	29
Figure 17: Proposed mutualized OFDM pilot position	30
Figure 18 - Propose common Tx architecture: $f_{IF} = \frac{B}{2} + \varepsilon$, $f_{RF} = 240$ GHz	31
Figure 19 - Proposed common Rx architecture: $f_{IF} = \frac{B}{2} + \varepsilon$, $f_{RF} = 240$ GHz	31

1 Introduction

This deliverable proposes to find a potential common architecture between wireless radio and wireless optical transmission that will allow us to mutualize as much as possible the processing in order to reduce the form factor of the modem. Indeed, in our first set-up and demo we planned to duplicate the radio and optical modems for transmitting the same Virtual Reality (VR) service.

Our study relies on the same assumptions that have been described in the WORTECS D3.1 deliverable [1] even though the 240 GHz RF band has been considered instead of the previous 60 GHz one. The analysis still considers the transmission of a VR video in the indoor environment cave. Therefore, starting from the analysis of the propagation channel characteristics for both systems, we first analyse the choice of the modulation format, taking into account also constraints of the hardware components, which are going to be used in the system. Indeed, channel characteristics show that a quasi LOS channel exists at these frequencies inducing no multipath propagation/fading. Therefore, ISI is negligible leading naturally to the choice of single carrier modulation scheme use. Nevertheless, considering the complexity implementation between OFDM and SC, the standards evolutions especially on optical communications, OFDM is selected in order to maximise the mutualisation of digital signal processing.

Both analog and digital radio and optical systems are described at the transmitter and receiver sides. The main functionalities that compose the digital PHY layer are explained including some of their limitations.

In conclusion, aggregating the reflection we exposed, we propose three main possibilities for mutualizing the radio and optical transmitter platforms. The proposal tries to push the mutualisation at its extreme by choosing a set of parameters matching for both radio and optical system with the more common components.

2 Propagation channel characteristics

The system parameters definition is mainly deduced starting from the propagation channel characteristics. Indeed, a signal transmitted over-the-air suffers from different variations that depend on several parameters such as: the carrier frequency, the signal bandwidth, the environment, the transmit power, etc.

The analysis below aims at extracting the main characteristics about the optical and 240 GHz radio channels that will be crucial for the design of both optical and radio systems.

2.1 Optical channel

Indoor light propagation is generally modelled using Ray Optics due to the small wavelength of optical frequencies. Assuming that the modelling objective is to find an approximation to the channel impulse response, which defines both channel gain and bandwidth, Monte Carlo Ray Tracing is the most used family of techniques due to the complexity of the scenarios. The simple equation that MCRT methods solve in Optical Wireless Communications (OWC) is the following:

$$P_{rx} = \int P_{tx}(\Omega) d\Omega$$

Where Ω is the emitter's output solid angle. The main problem to solve is the complex relationship between the emitter's output solid angle that impacts on the receiver, the multiple surface reflections, and time. Barry and Khan [2] proposed the first channel impulse response calculation method, which was deterministic with exponentially increasing complexity with the number of considered reflections. Classical Monte Carlo integration of Barry's approach obtained accurate estimations but needs a huge amount of rays. Importance sampling was further included in [3], using the transmitter's emission pattern and each surface's reflectance as probability density functions in the ray generation stage. This method improved convergence as the most energetic contributions are considered with more probability. Nevertheless, these methods' performance is subject to the impact probability on the receiver, which is generally of reduced size. In [4], Lopez-Hernandez et al. proposed a modification, including "forced" contributions after each reflection (line-of-sight contribution). This small modification sped up the calculations dramatically. On the older methods, random ray generation tried to perform both exploration (impacts on different part of the scenario) and exploitation (impact on the receiver and hence, effective contribution to the impulse response) of the scenario. On the other hand, modified schemes achieve exploitation in a deterministic manner, whilst exploration is still made using importance sampling. A new scheme based on Hamiltonian mechanics, concretely on Markov Chain Monte Carlo, was presented in [5]. In this work, the authors carried out the simulation of the CIR using an adaptive Monte Carlo integration governed by a Markov Chain. The system adapts automatically to the paths which transport more energy.

In WORTECS project, a Modified Monte Carlo scheme has been developed. However, the implemented simulator stores each arriving ray trajectory (to offer flexibility on the post-processing) and adds LOS contributions after each reflection simultaneously on all the pre-defined receiver points, increasing both flexibility and performance. Figure 1 depicts the simulation scenario and the ray tracing scheme.

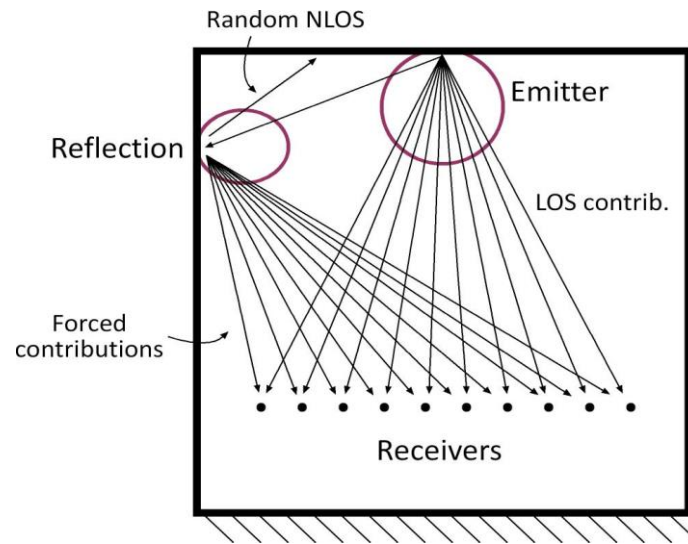


Figure 1 - WORTECS Ray Tracing scheme

In OWC, channel gain is generally defined by both emitter and receiver directivities. However, the most directive the emitter and receiver are, the lower the coverage area is. Regarding bandwidth, the channel impulse response enriches as the emission takes into account more solid angles, increasing frequency selectivity. Nevertheless, the most important parameter regarding bandwidth is the receiver’s FOV.

WORTECS demonstration scenario is characterized, from the OWC point of view, by 3 different surface types (Figure 2). These surfaces present diffuse reflection patterns at NIR and will not affect bandwidth significantly as it was shown in [1].

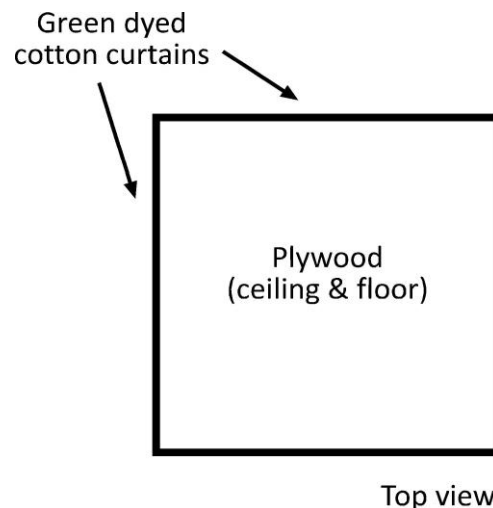


Figure 2 - Materials involved on the scenario

The proposed transmitter, in order to reach the 1 Gbps data rate objective of the first demonstrator, is based on OMEGA project’s NIR decoherenced-laser-plus-diffuser emitter [6]. This emitter provides eye safety, enough transmission power in a significant solid angle (30 degrees FWHM), and speed.

The simulations carried out in [1] revealed the necessity of including a stabilization mechanism on the HMD receiver due to the high sensitivity of the received power with the head movement. This result is complementary to the simulations carried out by Miramirkhani et al. in [7]. In their work, the authors demonstrated that the received power variation can be significant and proposed the use of adaptive techniques in the reception stage. Their proposal is based on considering a combination of lamps from where taking the signal, and the modulation depth for maximizing the SNR and spectral efficiency. However, their scheme would need from several complete demodulation chains, dramatically increasing both cost and complexity. In WORTECS, the receiver will be 2-axes stabilized and a handover strategy will be implemented to ensure full-time connectivity.

Furthermore, the resulting coverage area, which is primarily determined by the receiver's FOV (30 degrees FWHM), was about 1.5 m². The RMS delay spread among the coverage area defined by the receiver's FOV was estimated around 20-30 ps using the developed simulator. It can be concluded that the channel will introduce no limitations in terms of SNR or bandwidth within the coverage area.

In [8], typical OWC channel impulse response and delay spread values are also given for indoor environment considering LOS propagation and different distance and data rate between the transmitter and receiver. RMS delay spreads up to 2 ns are registered in some configurations.

2.2 240 GHz radio channel

The VR scenario use case, explained in details in [9], is intended to be an indoor scenario. Indoors, RF signals are usually propagating using multiple paths due to the presence of many reflective surfaces. Therefore, a multipath rich channel is expected for this use case.

Nevertheless, the initial analysis in [1] shows that due to the low transmit power and high path loss the link budget would be very poor. In order to compensate for the poor link budget, a solution, which we are going to pursue, is to use high gain antenna arrays. The analog front-end (AFE) should also support beam steering in order to be able to achieve coverage of users in the VR room. The beam steering is needed since the high gain antenna would produce a pencil beam, covering very narrow area. Therefore, the users should be tracked in order to obtain significant signal power at the receivers and therefore significant data throughput.

Since narrow pencil beams would be used, both at the access point and at the user, multipath propagation, i.e. non-direct path, components would be minimized, if any present at all. Even if some multipath components appear at the receiver, they would be significantly attenuated and, therefore, would not necessarily affect the system. Therefore, our propagation channel at 240 GHz in our VR environment demo has the main characteristic to be LOS as in OWC environment.

Due to the strong free space attenuation, narrow antenna beams and almost non-existence of multipath propagation, the channel model is expected to be frequency flat. In Figure 3 [10], the specific attenuation due to atmospheric gasses is shown. The region of interest is marked with a red transparent bar. As can be noticed from the standard curve, the attenuation for the region of interest is 2-3 dB/km. Since our use cases foresee communication distances of only a few meters, the attenuation would be way below 1 dB for different frequencies. It can be therefore assumed that the attenuation due to atmospheric gasses would not significantly affect the channel flatness.

Another effect that can be observed in dispersion of the radio waves at these frequencies. More details can be found in [11]. As can be noticed in [11], dispersion affects the path loss exponent on different frequencies. Nevertheless, this dependence is not significant, leading to almost frequency flat channel.

It is worth mentioning here that for the upcoming final demonstrator, use of a single channel of 10-20 GHz in the 240 GHz band would not be possible. The main limitation is that the commercially available data converters, analog to digital (A/D) and digital to analog (D/A), are not available. Therefore, covering the whole channel of 10-20 GHz with a single data converter is not possible for a real-time demonstration. In order to have a real-time demo, one approach would be to split the large channel in many smaller channels, e.g. 2 GHz each, and to use a separate baseband processor for each of them.

In order to transmit data using the whole 10-20 GHz channel, some off-line tests can be performed. Instead of using commercial D/A converter, an arbitrary waveform generator (AWG) can be used and instead of commercial A/D converter, an oscilloscope can be deployed for sample acquisition. There are commercial AWGs and oscilloscopes that do support bandwidths larger than 20 GHz. The frames to be transmitted would be prepared offline and using the AWG would be transmitted, while the received signal would be acquired using the oscilloscope. Decoding of the received frame would be again performed offline. This approach cannot be used for live demo, but its main purpose would be to show that transmission of multi-gigabit data streams over 240 GHz links is possible.

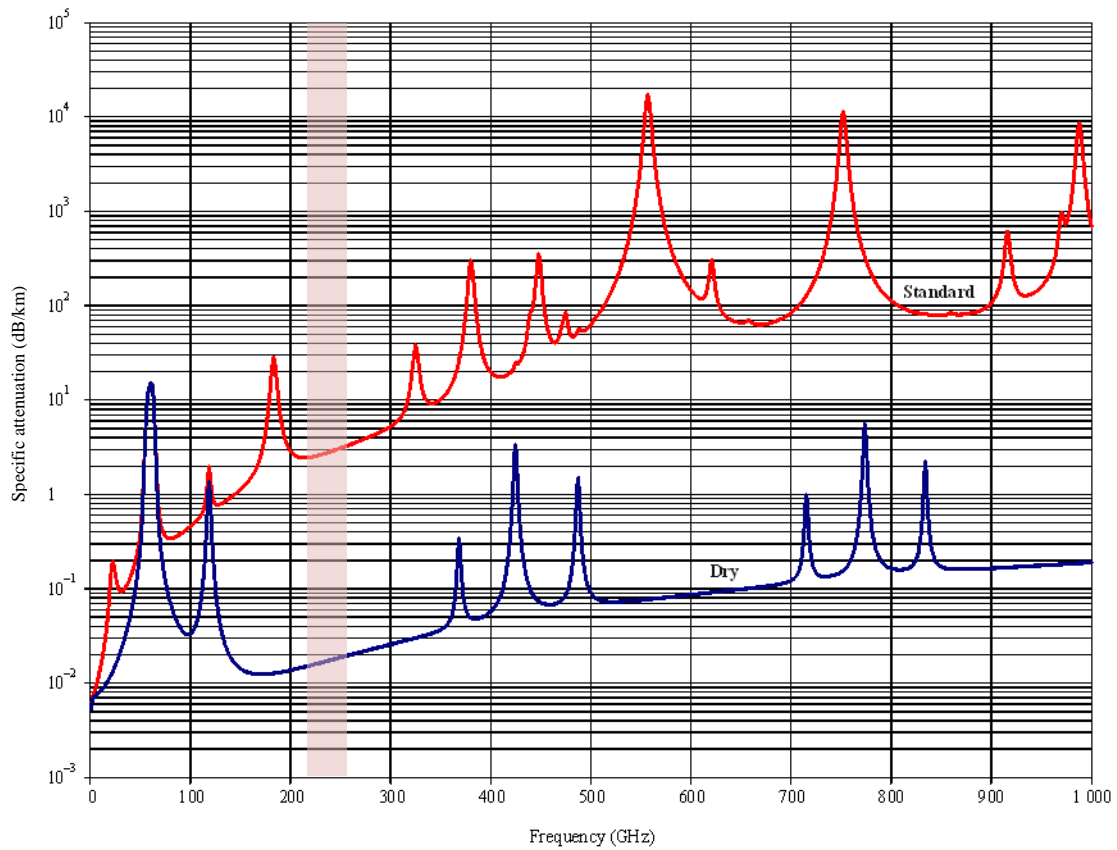


Figure 3 - Specific attenuation due to atmospheric gases, calculated at 1 GHz intervals, including line centers; ITU-R model

[11] confirms that at 240 GHz, the channel is viewed as LOS. Some measurements have allowed to model the channel and to extract its main characteristics. Indeed, channel impulse responses are recorded showing a fast decrease of the received power. In [12], typical delay spread values have been measured in indoor LOS environment that gives values up to 4 ns.

2.3 Radio and optical common channel parameters

The above descriptions of both radio and optics propagation channels show that common features can be considered. Indeed, in our indoor environment set-up demo with focusing transmission, the direct view between transmitter and receiver can be modelled (LOS) reducing the multipath and frequency channel selectivity. Typical measured delay spread values are quasi-similar between radio and optic transmission and in the range of 1 to 4 ns. Taken in consideration a mean of 2 ns, we obtain the coherence bandwidth defined by [13]:

$$b_{coh} = \frac{1}{2\pi\sigma_{rms}} \sim 80 \text{ MHz}$$

This indicator allows us to quantify the subcarrier spacing to choose in order to consider no variation (flat fading).

Another parameter to take into account is the coherence time that corresponds to the invariance of the channel in time. It is directly linked to the Doppler frequency (user speed).

$$t_{coh} = \frac{1}{f_{dmax}} = \frac{c}{f_0 v} \sim 1 \text{ ms}$$

with c being the light velocity ($3 \cdot 10^8 \text{ ms}^{-1}$), f_0 the carrier frequency ($240 \cdot 10^9 \text{ s}^{-1}$) and v the user speed (1 ms^{-1}).

These main characteristics should give advantage of using Single Carrier modulation instead of OFDM multicarrier one. This point is discussed in next Section 3.

3 SC vs OFDM

In Section 2.2, the channel model at 240 GHz was discussed. As it was concluded, it is expected a significantly frequency flat channel at this band. This would be especially valid if high gain phased antenna arrays are used, forming a pencil beam radiation pattern. As already noticed, the link budget is quite low, leading to the implementation of high gain antenna arrays in order to be able to transmit over the planned distance for the given scenarios.

Because the channel is almost flat, channel estimation and equalization would not be necessary at all. Having a frequency flat channel means no special requirements for the choice of modulation coding scheme (MCS). Therefore, choosing the simplest modulation would be the right choice. In this case a single carrier MCS would be the best choice. Support of different constellations would be needed in order to be able to adaptively change the data rate depending on the available SNR, which depends on, among other factors, the distance between the transmitter and receiver.

The channel is expected to be frequency flat, but that would not be the case with the AFE frequency response. Indeed, at high 240 GHz frequencies, it is challenging to design an AFE with a flat frequency response. This is due to the low quality of the passive components (resistors, capacitors, inductors, transformers, etc.) being implemented on chip (in silicon) at high frequencies. The Q-factor (quality factor) is quite low and cannot be improved if the used components are implemented on silicon. The usual choice is to use external, off-chip components for the critical parts of the AFE, because they have much better characteristics. Nevertheless, there are no external components for 240 GHz commercially available. Additionally, taking the signal off-chip and bringing it back on chip, using bond wires or bond bumps would introduce significant attenuation of the 240 GHz signal. Therefore, the AFE should be integrated on a single chip. This means that there would be no flat frequency response and probably additional impairments. In order to alleviate this problem, further compensation circuits are usually implemented on-chip. These compensation circuits improve the frequency response, as well as the impairments. Nevertheless, it is challenging, almost impossible, to fully compensate the frequency response and the impairments of the AFE.

Because compensation of the AFE non-linearities and impairments in analog domain is quite hard, the less costly approach is to perform the corrections in digital domain, i.e. in the baseband processor. The AFE frequency response can be estimated and the transmit power can be respectively changed, in order to compensate these impairments. The frequency response can be previously measured or can be estimated by the baseband. Channel estimation methods can be used to estimate the frequency response of the AFE. In theory, these can be estimated only once, but in practice, it can happen that the frequency response changes due to temperature changes. Therefore, standard channel estimation and equalization methods can be deployed in order to correct the AFE frequency response.

One problem, which appears with the single carrier modulations, is that the channel equalization can be significantly complex. The equalization is performed using a filter (e.g. FIR), which performs channel inversion to compensate the variations. For a low data rate system implementation such an equalization is straight forward. Nevertheless, in high data rate systems, implementing filters with multiple taps, can require a significant effort due to the high sample rates needed to be processed by the filters. These high sample rate streams are usually processed in parallel. Filters used for compensation should be also implemented in a parallel fashion which requires a significant effort. Therefore, a common approach is to use OFDM modulation [14], because the equalization in OFDM is performed using multiple single tap filters. This way, the required processing is significantly simplified. Additionally, with these multiple single tap filters, a frequency dependent IQ imbalance can be easily corrected.

From the discussion above, it becomes obvious that at these higher frequencies, use of OFDM has significant advantages and, therefore, it is going to be used for the demonstrators being planned in this project. It should be also mentioned that OFDM is sensitive to frequency offset and phase noise. Nevertheless, the frequency offset would be corrected using standard methods by using periodic pilot symbols in specific carrier frequencies at each OFDM symbol. The effects of phase noise can be minimized in a few different ways. First, a high quality, low phase-noise oscillator can be used. They are relatively expensive, but with development of the technology, different low-cost alternatives are appearing on the market. Additionally, the loop bandwidth of the used PLL can be additionally optimized in order to keep the phase noise to minimum [15].

The OWC introduces to main challenges in the design of the baseband system, i.e. the limited bandwidth of the LEDs (as the main component in the optical transmitter front-end), and the FIR filters in the system. In this case, using a multicarrier waveform is advantageous due to: firstly, it can adapt easily to the frequency response of the front-end and provide the best possible data-rate/BER performance. Secondly, assuming the effect of multipath to the system is negligible, because of the FIR filters in the transceiver chains, the received signal suffers from ISI which can be easily combatted when using OFDM waveform. In addition, the standard OFDM advantages, as discussed above, are enjoyed, namely the simplicity of the receiver architecture, and its spectral efficiency.

In sum, considering that radio at 240 GHz and optical communications are LOS, the utilization of a SC based transceiver seems reasonable at first glance. Nevertheless, due to using wideband signals at such frequencies, various nonlinearities could be compensated only using heavy computation resources, leading to the same order of complexity of an OFDM system.

Therefore, considering implementation efforts, the utilization of OFDM is well suited and would be considered on both wireless radio and wireless optic transmission. This way the intrinsic OFDM advantages, i.e. spectrum efficiency and equalization simplicity, will be maintained as well.

4 Analog front-end

With the current development of data converter technology, analog to digital and digital to analog converters, supporting more than a few GSps are rarely commercially available. However, there are application specific data converters which support tens and hundreds of GSps [16], but they are mainly used in oscilloscopes and/or arbitrary waveform generators. Additionally, a few data converters with sampling rates over 10 GSps has appeared on the market [AD, Fujitsy], but due to limited offer of support in the form of development boards, they are still not the best choice for research. Therefore, in this project we are working with proven data converters, supporting only a few GSps. In order to achieve multi-gigabit data transmission we are planning to use multiple channels bonded in one large channel. For each of these smaller channels, one baseband processor would be used. Each of them would transmit on a separate channel. The data converters would have in-phase (I) and quadrature (Q) signals.

4.1 Description & limitation both Tx and Rx radio front-end

4.1.1 Description of the Tx and Rx radio front-end

The RF front end delivered by IHP is planned to be a beam forming front end. It consists of an array of N-elements (e.g. 4 or 8) on a same chip. On-chip antenna is to be utilized, in order to avoid the need for interfaces between the chip and the antenna. These interfaces should work on frequencies above 200GHz and their implementation is a challenging task. By assembling, several units of this chip on a board a larger array can be constructed.

The initial plan for the antenna array is shown in Figure 4 with 4 elements assumed per chip. The final decision of number of elements per chip would be made as the chip top-level layout is in a more advanced stage and the available chip area would be known. Double folded dipole antenna would be used, a design which was previously silicon proven. With such a configuration, a $2 \times N$ or $4 \times N$ array can be demonstrated.

The AFE chip would have standard interfaces for the baseband signal. There would be 2 analog inputs, one for the in-phase and one for the quadrature signal. The bandwidth of each signal, in-phase and quadrature, should be less than 10 GHz. The input voltage range would be such that they can be interfaced to A/D and D/A converters, using simple attenuators. The inputs would accept differential signals, but can be easily converted to single ended signals using balun transformers.

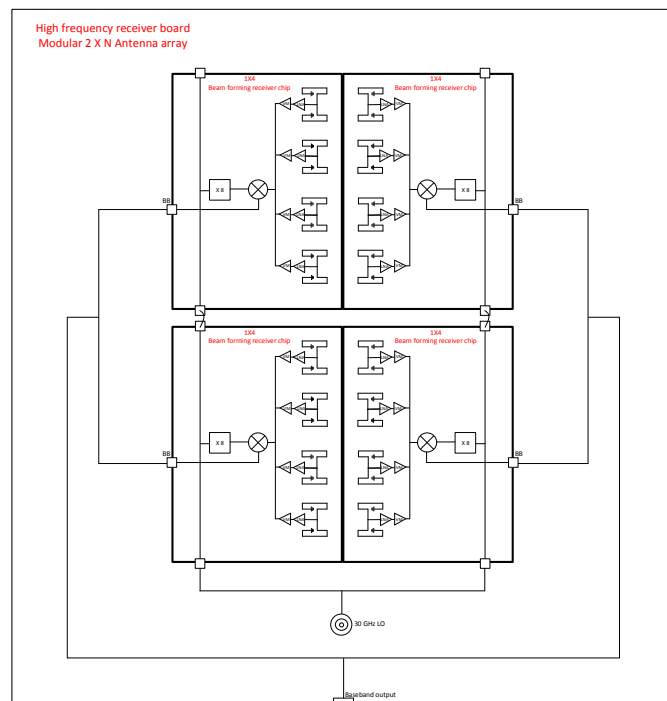


Figure 4 - Initial plan of the antenna array configuration

4.1.2 Limitation of the Tx and Rx radio front-end

Many challenges or limitations exist at this point regarding the development of the analog frontend. These challenges are mainly on component level as well as on overall chip architecture level. Some of them were already sorted out and resolved, but some would be investigated and resolved later.

From the component point of view the elevated minimum noise figure and declined maximum available gain at such frequencies puts a huge constraint on the link budget. The reduced output power limitations has been improved by designing a power combining power amplifier. Other limitations, such as the resultant bandwidth after cascading all the blocks, would be quantified after finishing the top-level design of the overall transceiver.

From the overall chip architecture point of view some challenges are to be faced regarding the tolerances of the dicing of each chip. This would affect spacing tolerances between the chips and, therefore, the antenna element spacing in the final phased antenna array.

Another challenge is the routing of the LO and baseband signals in terms of matching requirements on board and in terms of signals losses especially for the LO signal. Such losses must be compensated on chip.

The coherence between the LO signals across different chips should be monitored. This limitation can be solved by careful routing of the LO signal across the board. Additionally, adding vector modulator on the LO path can drastically improve the introduced phase mismatch.

Further challenge and design decision are the architecture of the control circuitry for the used vector modulators. The possible solutions include having an SPI for each chip, or having a common control unit for all the chips available on a single board.

All these challenges are being investigated. The solutions that are found are being thoroughly analysed and simulated and if they satisfy the minimum requirements, they are implemented in silicon.

4.2 Description and limitations of both Tx and Rx optical front-ends

The OWC transceiver used in this demonstrator consists of two main parts: a) Transmitter. An infrared (IR) laser with modulation capabilities and power adjustment up to OWC needs operating in a health safety mode. This laser can be easily modulated at 250 MHz, a frequency defined as sufficient to transmit at a with an spectral efficiency of 4 bits per Hertz. b) Receiver. The second element is the photodetector, this element is critical because of its small active area challenges the optical flux harvest. Nevertheless, its cut-off frequency makes it to operate with the Tx laser.

4.2.1 First OWC Demonstrator

The Optical Transmission Head (OTH) circuit uses an infrared (IR) laser. The laser is used to obtain a maximum 100 mW power as concluded from the scenario modelling. To avoid any dangerous laser radiation power, a sanding diffuser is set in front of the laser to break the laser coherence. The Optical Detector Head (ODH), i.e. the light collector and the photodiode uses an Avalanche Photodiode (APD) [6]. Radiometric losses due to solid angle distribution in emitted energy and small size sensing area of the APD urge for the use of an adapted optical concentrator. From modelling, transmission distances of 2 m and 1.5 m are taken into consideration. The emitting laser source has a Lambertian behaviour and its losses are foreseen at -44 dBm for an angle of 30 degrees. Thus, the optical concentrator design takes 30° of angular acceptance as design parameter. Given the 1 Gbps data-rate target of the first optical demonstrator, a bandwidth of 250 MHz will be used.

4.2.2 Block diagram of transmitter design

Figure 5 depicts the basic configuration of WORTECS transmitter that integrates a laser source.

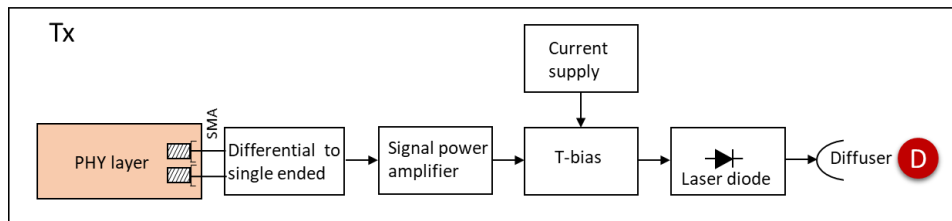


Figure 5 - WORTECS basic transmitter.

Tests recently carried out by partners on various commercially available laser diodes show that the cut-off frequencies are between 250 MHz and 400 MHz. Constant current laser source is specified in Table 1. T-bias allows the modulating signal to pass through the laser. This signal arrives in a digital format to a digital-to-analog converter (DAC), the DAC is in the PHY layer. This last will deliver analog signal to a differential-to-single ended stage. A compensator (optional) allows to linearize the signal just in case of transmission rate loss. Prior to T-bias we find the signal power amplifier. All components work in the modulation band of IR laser diode (250 to 400 MHz). A transmission rate of 4 bits per Hertz has been decided (Schematic of analog transmitter is in Fig 60, Appendix A2 of D3.1 [1]) which will permit to obtain a data rate of 1 Gbps.

Table 1 - Main optical Tx components

Component	MAX4444/5 Differential line receiver	AFT05MS0 03N RF power LDMOS transistor	THS4304 Wideband operational amplifier	TAT7457 DE - 1200 MHz, 75Ω adj gain RF amplifier	LD1255R 250mA Precision constant current laser driver	RLT860M-250MG High power IR laser diode
Stage (Refer to Figure 5)	Differential to Single-ended conversion	Signal power amplif.			Current supply	860 nm Transmission light source

The Tx PCB appears in Figure 6. The couple of gold male connectors are MMCX, there is a micro USB connector and the connector in black the power supply entrance. The three main modules are shielded while the T-bias is visible directly on the card (left picture).

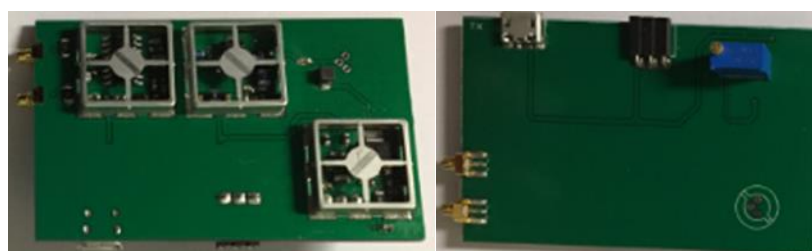


Figure 6 - Tx OFE PCB.

4.2.3 Second free form parabolic concentrator

The OWC Rx uses an APD (FirstSensor AD1900) previously tested in Omega project. The receiver has 30° FoV and its sensitivity is to be tested. The APD has a 3mm² surface and the irradiance flux arriving to its active surface is low. Increasing the entrance area permits to gather more irradiance flux. A 12 mm diameter anterior surface lens permits to have a 113 mm² area increasing substantially the power into the APD. Nevertheless, due to the acceptance angle required and the small APD sensing area a simple lens cannot be used. Instead a Free-form Optical Concentrator (FFC) was designed as shown in Figure 7. It guarantees that total internal reflections (TIR) conducts most of the first ray reflections into the active APD area. TIR avoids metallic thin films and extra production costs. Only a low amount of optical flux (marked in red in Figure 7) is lost in the edge of the exit surface of the concentrator. The lost rays correspond to a relatively small entrance surface (approximately 10% of the total entrance surface).

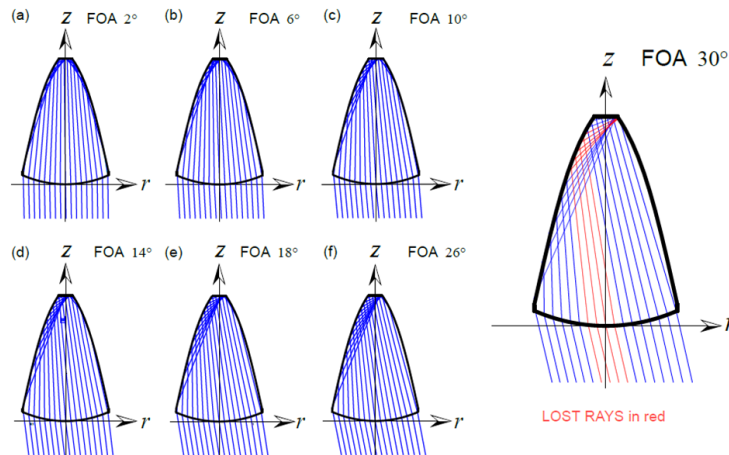


Figure 7 - WORTECS second version of the free-form optical concentrator. At 30° it experiences a small entrance ray losses.

This FFC will have a collection area equivalent to the Parabolic Compound Concentrator (PCC). The FFC conducts the incoming signal into the APD.

4.2.4 Block diagram of AFE Receiver (Rx)

In Figure 8, the first element is a DC-to-DC converter (marked as charge pump) that will polarize the APD. After the APD, a filter rejects noise and sends an adapted signal to pre-amplification. A second filtering stage will further clean the signal. A variable gain amplifier (VGA) permits to adjust output signal level. This can be digitally controlled directly from the PHY layer (refer to the schematic of analog receiver is in Fig 61, Appendix A2 in [1]).

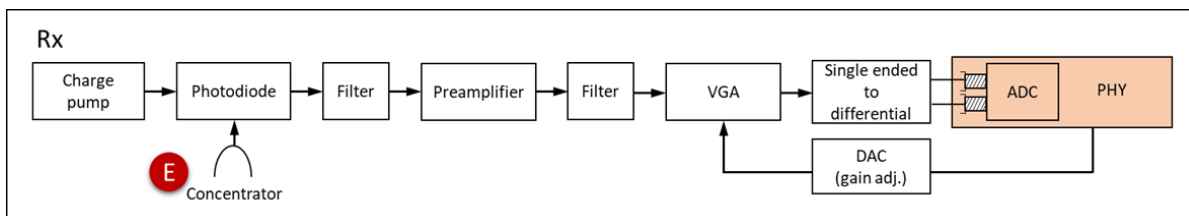


Figure 8 - WORTECS Rx Optical Front End.

Table 2 summarizes main components for AFE. After arriving FFPC light is focused into an Avalanche Photodiode (APD). Two APD are retained. First option is AD1900-8 TO from First Sensor (already used in Omega project). Even if this APD is frequently out-of-stock, a supplier has been selected as the photodiode for this project because of its price, higher bandwidth and assessment. Given its breakdown voltage the APD needs a regulated high voltage DC-to-DC converter. The selected device from EMCO, is depicted in figure 9 and its function appears in Table 2.

Table 2 - Optical Rx components

Component	AD1900-8 TO (First Sensor)	C02 (EMCO) Low noise, high voltage power supply	THS4304 Wideband Operational Amplifier	AD8367 Linear-in-dB VGA + MAX5141/4 DAC	THS4541 Differential Amplifier
Stage (refer to Figure 8)	Light-to-current conversion	Regulated high voltage DC to DC converter (charge pump) for APD.	Filtering and Preamplification	Variable Gain Amplification + DAC for gain adjustment	Single-ended to differential amplification

Filtering stages are used to filter out DC and switching frequencies from DC-to-DC convertors; a preamplifier is preparing the analog filtered signal for it to meets the requirements of the next stage for further processing. A second filtering stage filters out RF frequencies. The Variable Gain Amplifier permits to prevent the signal from saturation while providing the required gain. From PHY layer, a digital signal is sent to VGA for this last to adjust the gain. An additional DAC is used to convert this digital signal in an analog input for VGA. The final stage consists in a single-ended to differential to prevent GND be used as reference.

The main challenge comes from the receiver stage because of the free space loses that are expected. This will be the first time a link at such a transmission rate (at a frequency of 250 MHz) and range >1.5 m will be tried. Fast redesign time for blocks in the Rx is critical, so to reduce fail probability some commun tests will be carried out between pureLiFi and Oledcomm.

5 Digital baseband

5.1 Description of both Tx and Rx radio digital baseband

The key focus of the digital baseband processor is to realise low-complexity and low-power architecture for ultra-high throughput and low latency radio link from the VR server to the user’s head mounted display (HMD) leveraging the large frequency resource of the THz band in general and carrier frequency of 240 GHz. The key aspects/elements of the baseband architecture have been covered in this section. Detailed specifications and values will be drawn in view of the measured performances of transmit and receive AFEs and the resultant hardware impairments. The envisioned architecture has been presented in the following sub-sections. First, the overall architecture of the baseband processor (modem) is described and further, for each of the blocks, a short description is presented. The possible solutions are listed and most preferable parameter values are presented.

5.1.1 Channel bonding

As mentioned earlier, use of data converters supporting tens or hundreds of GSps is challenging. Therefore, we decide to utilize data converters supporting just a few GSps and to transmit on multiple neighbouring sub-channels.

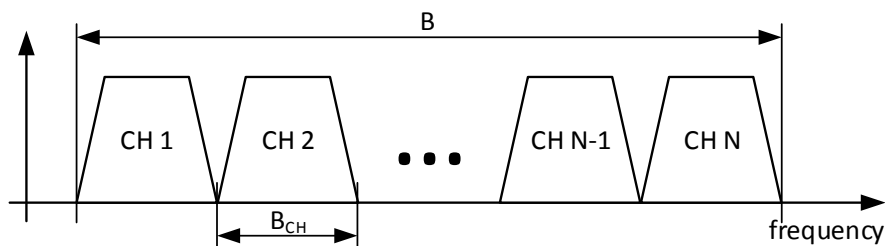


Figure 9 - Multiple neighbouring sub-channels exemple

In Figure 9, multiple neighbouring sub-channels, forming a larger channel is shown. Each of the sub-channels have a bandwidth of B_{CH} and the channel has a bandwidth of B . Minimum spacing between the channels is B_{CH} , but usually a guard interval between the channels should be present. In case of a guard interval with bandwidth of B_G is used, and N sub-channels are deployed, the overall bandwidth would be

$$B = N \cdot B_{CH} + (N - 1) \cdot B_G \quad (1)$$

With this approach, depending on the number of sub-channels N , different channel bandwidths can be achieved. This is a scalable design which can be used to achieve arbitrary channel bandwidth and, therefore, arbitrary data throughput, by using commercially available data converters. The baseband can be implemented on a programmable hardware, i.e. FPGA, as well as on and ASIC.

5.1.2 Digital Baseband Architectures

As mentioned earlier in Section 4, OFDM is chosen for the envisioned use cases and, at the same time, is the most commonly known and applied multi-carrier scheme. It has been adopted as the baseline for the state-of-the-art radio access technologies such as LTE and Wi-Fi IEEE 802.11. The main benefits of the OFDM system are reduced equalization complexity from the use of cyclic prefix (CP) being to handle multipath fading channels, and, consequently, an efficient multiple-input multiple-output (MIMO) processing support. However, its good performance is valid only when synchronization and inter-subcarrier orthogonality are strictly preserved [17]. With OFDM, the ISI created by multipath propagation can be suppressed using CP, if the length of CP length exceeds the delay spread of the channel. Despite the fact that OFDM provides a high spectrum efficiency, it suffers from OOB (out of the band) emissions due to digitally filtering the whole bandwidth with Sinc pulses.

In order to avoid the above OFDM limitations, filter-based waveforms have been widely studied. This includes various filtered OFDM variants where filtering can be performed from the subcarrier level to a sub band level (e.g., a resource block in LTE). The filter is designed to have a more suitable shape with reduced side lobe levels. This would relax requirement on strict synchronization by supporting asynchronous transmission [18].

Filter-bank multicarrier (FBMC) is a subcarrier filtering based waveform that includes a pulse shaping functionality on a per subcarrier basis [19]. Due to its filter design, FBMC side lobes are much smaller compared to OFDM thus the ICI issue is very small. FBMC adopts no ISI mitigation scheme as CP is not used. The per-subcarrier filtering feature makes FBMC robust against carrier frequency offset (CFO) [20]. It is also observed in [21] that due to the per-subcarrier filtering, the tail of the filter's impulse response in FBMC systems will typically cover four symbol intervals. This makes FBMC not suitable for small packet transmission and low latency applications unlike OFDM in which, data transmission and reception can occur within a symbol interval.

Universal filtered multi-carrier (UFMC) is another type of sub-band filtering-based waveform, where only a transmit filter is used while the demodulation in the receiver relies on the discrete Fourier transform (DFT). In order to prevent any inter-symbol interference (ISI) due to the filtering operation, zero prefix (ZP) is typically used in UFMC, instead of CP. The typical filter length of UFMC is less than or equal to the length of ZP. Therefore, the filter tails extend into the ZPs without overlapping with each other [22].

A summary for different waveforms is depicted in Table 3 below. The findings of literature survey can be summarized as follows: multicarrier based new modulation candidates FBMC and UFMC achieves lower OOB emissions than the standard OFDM even in the presence of PA nonlinearity. Standard OFDM outperforms new filtered-based waveforms in terms of BLER since ISI has been completely removed. The filter-based waveforms will lose small BLER performance compared to that of standard OFDM due to the extra ISI. In particular, UFMC loses BLER performance against OFDM in high SNR region. The degradation is more severe for high-order modulation because the dense constellation makes it more sensitive to the interference [20]. UFMC has the worst performance due to extra noise enhancement caused by FFT operation [20]. The key advantage of OFDM is that it can greatly simplify the receiver design through utilization of single-tap equalizers. The receiver structure of UFMC is similar to that of standard OFDM. Therefore, traditional channel estimation and equalization techniques can be directly used. However, channel estimation and equalization in FBMC is less explored than in traditional OFDM systems [20]. Similar to the traditional OFDM, FBMC and UFMC also have a large PAPR [23]. According to [22], it is difficult for FBMC to support high-order modulations even with more complex receiver structure.

Table 3 - Summary for different waveforms, grades A to C indicate good to bad. [20]

Waveform \ Metrics	OFDM	FBMC	UFMC
Filter granularity	whole band	subcarrier	subband
OOB without PA	C	A	B
OOB with PA	C	B	B
Low latency	A	C	A
BLER vs SNR	A	B	C
CFO robustness	B	A	B

PA denotes power amplifier nonlinearity.

5.1.3 Orthogonal Frequency Division Multiplexing (OFDM)

According to the previous discussion, OFDM is the most favourable modulation. Due to limitations in the commercially available hardware, the large available channel bandwidth in the 240 GHz band is going to be split in multiple sub-channels. Depending on the chosen bandwidth of each of these sub-channels and available SNR a multi-gigabit throughput would be available on each of them. For each of the sub-channels, a separate baseband processor would be used. With the current speeds of the available FPGAs and most of the ASIC technologies it would be hard to implement the baseband processing using a single data path. Therefore, it is a common practise [24] [25] to implement the processing in multiple parallel data paths.

- **Transmitter**

The transmitter architecture is shown in Figure 10. It has a parallel architecture.

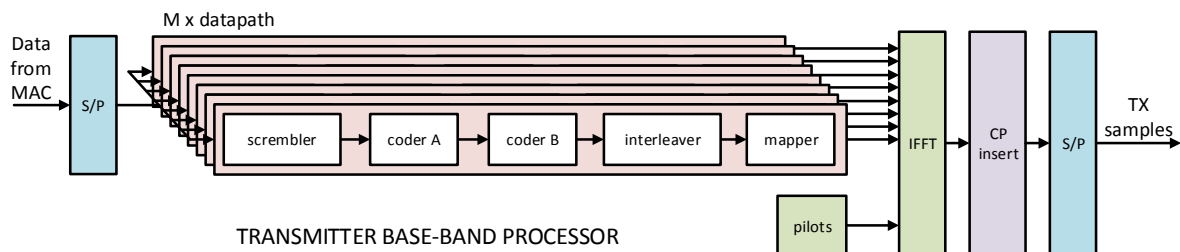


Figure 10 - Block diagram of a parallelized OFDM transmitter

Depending on type of FPGA/ASIC and the required data rate, M parallel data paths are used. In the next subsections, each of the components is described.

- **Serial to parallel (S/P) converter**

The data arriving in the baseband, from MAC, is assumed to be in a serial format. Before processing the data, it should be split between the available M data paths. Therefore, each successive M bytes/words are assigned to M available data paths.

- **Datapath**

The data path for the OFDM transmitter is consisted of scrambler, coder A, coder B, interleaver and mapper and an IFFT block. These parts can be easily parallelized. Using multiple parallel IFFTs is also possible, but this would increase the complexity, and would not improve the processing speed additionally. Nevertheless, there are quite efficient IFFT implementations and parallelizing it is not really needed.

- **Scrambler**

The data arriving from the MAC layer should be random. Anyway, there is no guaranty that this would be the case for the data arriving from higher layers. In order to avoid long sequences of ones or zeros in the incoming data stream, a scrambler, or randomizer is used to randomize the data arriving from the MAC.

There are basically two types of scramblers. The first is additive and the second is multiplicative. Additive scramblers add (binary) pseudo-random binary sequence (PRBS) to the incoming data sequence. Multiplicative scramblers, on the other hand, multiply its transfer function with the incoming data sequence. One main difference is in the descrambling. The additive scramblers need a reset for synchronization before the data is descrambled, while the multiplicative descramblers are self-synchronizing.

In the architecture proposed here, an additive scrambler is going to be used. The main reason is that there is already a synchronizer available at the receiver. This synchronizer would generate a pulse, on each arriving frame, and this pulse can be used for synchronization of the scrambler.

- **Coder A**

In order to improve the coding gain in one transceiver, a two stage forward error correction (FEC) is used. The first stage, called outer code, is usually a block code, usually a Reed Solomon code. The output of this coder is supplied in the input of the second coder.

- **Coder B**

The second coder, also called inner code, is usually a convolutional or LDPC code. According to [26] LDPC codes have better coding gain compared to convolutional. Nevertheless, resources needed for implementation of LDPC are much higher compared to convolutional codes. From this perspective, in high performance, multi-gigabit systems with limited resources, convolutional codes are preferred.

Additional discussion for the available and commonly used FEC is performed in one of the following sections.

- **Interleaver**

In order to obtain good code performance of the convolutional code, avoiding burst errors is necessary. The FEC would perform significantly well only if there are not too many errors in a given code word. Therefore, the errors should be dispersed through different code words. Usually, this is performed using an interleaver. The interleaver changes the order of the incoming symbols (or bits) and, therefore, a burst of errors is dispersed. There are mainly two types of interleavers: block and convolutional. In a block interleaver, the data is written to memory in rows and read out in columns. In a pseudorandom block interleaver the data is written in sequential order in a memory and read out pseudorandom order. In a convolutional interleaver, the incoming data is multiplexed into and out of a fixed number of registers.

The main disadvantage of the interleavers is the latency they introduce in the system. The latency depends on the length of the interleaver. The smaller the length, the lower the latency. Nevertheless, the length must be kept larger than a given minimum in order to have efficient FEC. In our system where the channel is quasi-invariant in time and frequency the interleaver would need to be quite long and introduce significant delay.

In a single carrier modulation coding schemes, the symbols (or bits) are interleaved in time. This is called a time interleaving scheme. In multicarrier modulation coding schemes like OFDM, the data symbols in one OFDM are interleaved. Therefore, symbol errors due to deep fade in one frequency are dispersed through the whole OFDM symbol and are not concentrated around one frequency.

As discussed previously, the channel is expected to be band limited AWGN channel. Since the link budget is quite low, high gain antennas are going to be used. This would lead to narrow antenna beams (i.e. pencil beams) which would eliminate multipath propagation. Since OFDM would be used and the analog frontend is expected not to have flat frequency response, a frequency interleaving should be used. This would disperse the errors caused by a frequency dependent attenuation. The dimension of the frequency interleaver should be equal to the number of data symbols in a single OFDM symbol.

- **Mapper**

The mapper simply maps the incoming bits to symbols and, in the case of OFDM, assigns these symbols to data subcarriers. Two possible mapping strategies are possible. First, same constellations can be used on all subcarriers, depending on the channel state, i.e. link quality and the required data rate. The second strategy is to use different constellations, depending on the link quality for each subcarrier. The subcarriers experiencing higher SNR can use higher constellations and the ones experiencing lower SNR can use lower constellations. This is also known as OFDM with multiple constellations (or OFDM-MConst) [27]. OFDM-MConst is a good

candidate, since the channel is expected to be flat and the analog frontend not to be frequency flat. Depending on the flatness of the analog frontend frequency response, one of the both mentioned OFDM schemes can be used.

- **Pilots**

Pilot carriers are needed to estimate the channel and perform system synchronization. In this case the channel is frequency flat bandlimited channel and no channel estimation is needed. Nevertheless, these pilots can be used to estimate the flatness of the analog frontend. If the analog frontends have same frequency response, than this step would not be needed. Anyway, due to process variations and due to large channel bandwidth of the channel at 240 GHz, it is quite likely that there would be variations between the analog frontends. Therefore, the pilot carriers can be used for estimation of the frequency response of the analog frontend.

The number of pilot carriers can be relatively small in this case, since the channel is not changing. The analog frontend frequency response can change due to temperature, but this change is relatively slow. Due to the slow change of the frequency response of the analog frontend, even a single pilot can be used for estimation of this frequency response. The pilot carrier position should be changed in each OFDM symbol, in order to estimate the whole channel bandwidth.

- **Inverse fast Fourier transform (IFFT)**

After mapping symbols to subcarriers, an IFFT is performed. The size of the IFFT depends on the channel coherence bandwidth. The smaller the coherence bandwidth the more subcarriers needed. In the case of 240 GHz, the channel is expected to be frequency flat. Nevertheless, the frequency response of the analog frontends is not flat and therefore it can be used as a starting point for selecting the number of subcarriers. In the 60 GHz band, our previous calculations show that 1024 subcarriers [28] would be enough for all the possible cases. This would be probably more than needed for the 240 GHz case, but it would be a safe option.

- **Cyclic prefix (CP) insertion**

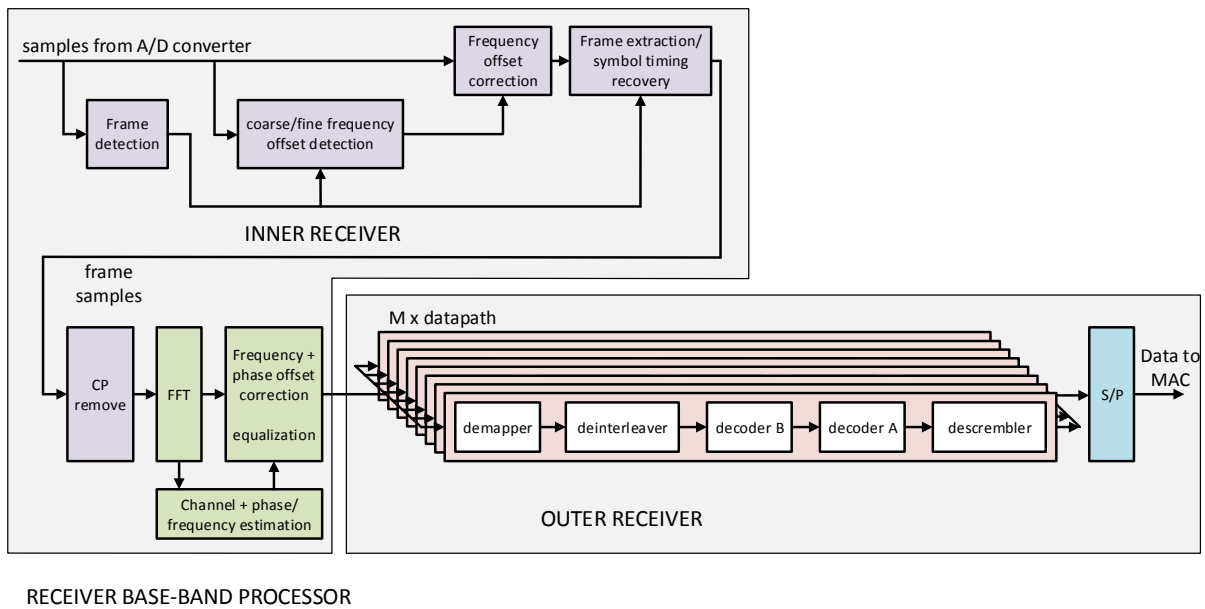
Due to multipath propagation an inter symbol interference is expected at the receiver. In order to mitigate the inter symbol interference a cyclic prefix is usually used in OFDM modulation schemes. Since no multipath is expected at 240 GHz, the cyclic prefix is not needed. Anyway, there are two reasons to use cyclic prefix. The analog frontend is not ideal. Therefore, there would be crosstalk between different paths of the received signal. This would be same as having a multipath. In order to mitigate ISI due to this crosstalk a cyclic prefix can be used. The second reason is to use cyclic convolution instead of linear convolution when processing the incoming signal.

- **Parallel to serial (P/S) conversion**

The parallel to serial conversion is used for serializing the data from the IFFT and sending it to D/A converter. In the radio transmitter, the real and the imaginary parts are split and sent to two separate D/A converters in order to create the in-phase and quadrature signals.

- **Receiver**

The receiver, compared to the transmitter, is slightly more complex due to the additional functions needed to be implemented. Typical multi-gigabit receiver architecture is shown in Figure 11. The receiver is split in two parts, called inner and outer receiver. The inner receiver performs synchronization and channel estimation and the outer receiver performs symbol demapping and FEC.



RECEIVER BASE-BAND PROCESSOR

Figure 11 - OFDM based receiver data-path

▪ **Synchronization**

The synchronizer is essentially performing three different tasks. First, it is detecting a frame arrival. Second, the coarse and fine frequency offset estimation and correction is performed, and finally symbol timing recovery.

In order to detect an incoming frame, a preamble is used. This preamble is positioned in front of the OFDM symbol and the frame header. The frame format, consisted of a preamble and an OFDM symbol is shown in Figure 12. The structure of the preamble is shown in Figure 13. As can be noticed the structure is periodic and this enables relatively simple frame arrival detection.

In order to detect a frame arrival, a so called delay and correlate algorithm is used. The incoming signal is correlated with a delayed copy of it, as shown in Figure 14. When a preamble containing a repetitive sequence in it arrives at the receiver, a peak with a plateau is obtained at the output of this block. This peak is used for frame arrival detection. After a frame arrival is detected, coarse frequency offset estimation and correction is performed. Further, a cross correlation with the long training sequence is performed in order to generate two cross-correlation peaks which are narrow and used for symbol timing extraction. This is performed after coarse frequency offset estimation since performing cross-correlation in presence of frequency offset can lead to unreliable results.



Figure 12 - OFDM frame format

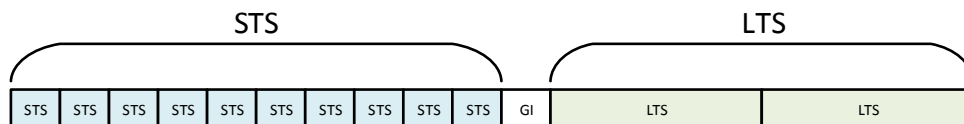


Figure 13 - Preamble format

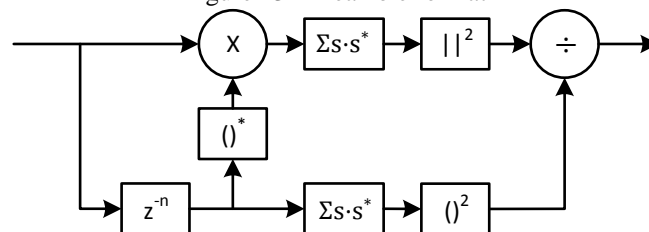


Figure 14 - Delay and correlate algorithm for preamble detection

- **Carrier frequency offset and phase offset estimation and correction**

Carrier frequency offset estimation and correction is needed because the local oscillators of the transmitter and receiver are oscillating in a slightly different frequencies. This can cause problems in the used algorithms for OFDM symbol timing recovery and can cause inter-carrier interference (ICI) between subcarriers in the OFDM symbol.

The frequency offset is estimated using the peak with the plateau on the output of the auto-correlator, i.e. delay and correlate block (algorithm). The phase of this plateau depends on the frequency offset. The frequency offset can be easily estimated using the plateau phase [29]. Since the frequency offset is estimated, it can be easily corrected using a numerically controlled oscillator and, usually, a CORDIC processor.

The phase can be estimated and corrected using the same cross-correlation peaks. This phase is the phase offset added to the signal of interest. The whole signal should be just multiplied by a normalized complex conjugate of the cross-correlation peaks used for symbol timing estimation.

- **Cyclic prefix (CP) removal**

Cyclic prefix is the only part being affected by the multipath propagation or by the ISI caused by the non-perfect AFE frequency response. It is simply removed before further processing takes place.

- **Fast Fourier transform**

FFT is used to convert the time domain signal to an OFDM symbol. Further, the symbols in the subcarriers are demapped.

- **Channel estimation and equalization**

In OFDM receiver, the channel is estimated by using pilot subcarriers inserted in the OFDM symbols. These pilot subcarriers have known amplitudes and phases. The positioning of the pilots can be fixed or can be changed for each OFDM symbol. The number of pilots can be chosen depending on the expected time and frequency coherence.

Since in our case the channel is stationary and frequency flat, the number of pilots can be even reduced to a single one, which would change its position with each OFDM frame. After a number of frames are sent, many subcarriers would be sounded and the frequency response can be estimated. Since the channel is expected to be flat, if the frequency response of the AFE is relatively flat, this can be a good approach which would introduce only a small overhead.

- **Data path**

The data path takes the incoming samples decodes them in order to reconstruct the received data. The incoming samples are first demapped i.e. the symbols are converted to code words and, then, the code words are decoded. First the data is deinterleaved and then decoded. Depending on the used FEC coding, the decoder is respectively chosen. Further descrambling is performed and the received data is obtained.

- **Demapper**

The demapper performs the opposite function of the mapper. It takes the incoming symbols and generates the code words bits, later to be decoded using the decoder.

- **Deinterleaver**

The deinterleaver is used to combat the burst errors. In case of burst errors, the interleaver would spread them, allowing optimal performance of the FEC decoders.

- **Decoder B**

Depending on the used coder B, the decoder can be LDPC or Viterbi for decoding of convolutional codes. The decoder can be also a soft decoder in order to slightly improve the decoder efficiency.

- **Decoder A**

The decoder A is optional (also coder A) and it is usually a block coder. A Reed-Solomon is a common choice. Depending of the coder/decoder B, this coder/decoder can be used or bypassed.



- **Descrambler**

The descrambler is performing the inverse operation of scrambler. It multiplies the bits of the incoming sequence with a pseudorandom sequence in order to return them in a form in which they were before scrambling.

- **Serial to parallel (S/P) converter**

The serial to parallel converter groups the received bits in word in order to handle the received data to the upper layer (MAC) for further processing.

5.1.4 Forward Error Correction (FEC)

Forward error correction (FEC) coding helps to reduce the bit error rate. In other words, FEC, also known as channel coding, is used to withstand or minimise the error due to channel noise. For FEC, the transmit signal is coded in such a way that the receiver will be able to fix most of the errors introduced by the noisy channel i.e. errors can be corrected at the receiver without the need of retransmission. Broadly, channel codes can be categorised as convolution codes or block codes.

- Block codes: memoryless addition of redundant information
- Convolution codes: convolution of input with encoder's impulse response

At the receiver, hard decision decoding can be employed wherein the output of the channel is immediately converted to a 1 or 0 (hard decision) before being decoded to original information bits. Whereas for soft decoding, a scale of 8 to 16 levels (3 to 4 bits) is used to decide exactly how close to 0 or 1 an actual received signal was. This is often used in conjunction with a soft input decoding algorithm. Soft decoding outperforms hard decoding in terms of bit error rate (BER) but also increases complexity at the receiver. Reed Solomon code is an example of block code, which are usually decoded using hard-decision decoding. Convolution codes are simpler to implement for longer codes and soft decision decoding at the receiver is relatively easier as compared to block codes. Convolution codes are generated by passing a data sequence through a transversal i.e finite impulse response (FIR) filter.

As can be seen in Figure 15, above a certain threshold SNR cross-over point, the FEC coded BER performance is better than uncoded BER performance i.e. same BER can be achieved for a lower SNR. This decrease in the required SNR for a given BER performance as compared to the uncoded SNR requirement is termed as 'Coding Gain'. Coding gain is positive above the threshold/cross-over SNR 'X'. It is negative below the threshold/cross-over SNR and in that case there is no point in using FEC.

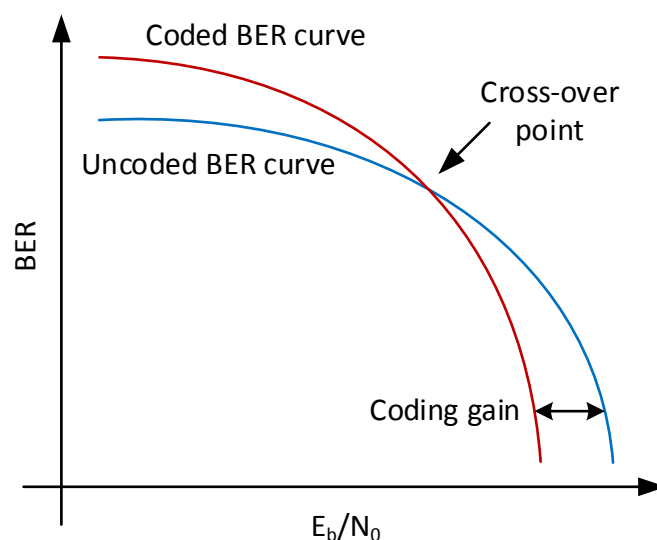


Figure 15 - FEC coding gain

Modern FEC codes include Low-Density Parity-Check (LDPC)/Gallager, turbo, and polar codes. LDPC codes are adopted in many standards for example, Wi-Fi (802.11n, .11ad, 5G NR) and DVB-S2 standard for the satellite communications. There are also some practical applications for turbo codes such as HSPA, LTE, and WiMAX. Polar codes are gaining much attention in the recent years since they are used in 5G NR specification for controlled signals.

1. Low-Density Parity Check (LDPC)

LDPC codes are a class of linear block code. The term “Low-Density” refers to the characteristic of the parity check matrix which contains only a few “1”s in comparison to “0”s.

Parameters: code length n , with k information bits, and an $m \times n$ parity-check matrix H .

An (n, k) block code takes k bits at a time and produces n bits and the code rate $R=k/n$.

- Possible parallel implementation of the decoder which leads to higher throughput
- For a given spectral efficiency, the LDPC code outperforms the RS code by roughly 3 dB (IEEE 802.3bn)
- Decoders: sum product algorithm (SP), belief-propagation (BP) decoding and bit flipping algorithm
- Disadvantage: error floor; conventionally the BER steadily decreases in the form of a curve as the SNR increases. Error floor is a point after which the curve does not fall as quickly as before
- Implementation example: a decoded throughput (T/P)= 78 Gbps and a latency of 0.06 μ s have been demonstrated in [30] for an LDPC code having a block length of $K = 1723$ and a coding rate of $R = 0.84$

2. Turbo

It is the concatenation of two convolutional codes separated by an interleaver. Hence, it can be concatenated either in serial, parallel or hybrid manner.

- Decoders: max-log approximation and soft-input soft-output (SISO) decoding
- Disadvantages: higher latency than the LDPC code due to usage of interleaver and it also suffers from error floor
- Implementation example: authors in [31] demonstrated a fully-parallel turbo decoder that achieves a decoded throughput of 21.9 Gbps and a processing latency of 0.24 μ s, for a turbo code having a block length of $K = 6144$ and a coding rate of $R= 1/3$

3. Polar

Polar codes are currently under consideration for potential adoption in future 5G standards. They are constructed as a result of the channel polarization transform.

- They have a very low error-floor
- Decoders: successive-cancellation (SC) decoding, successive cancellation list (SCL) decoding, and belief-propagation (BP) decoding
- Disadvantages: polar codes are not universal due to dependency on the underlying channel. If a channel is unknown to a transceiver, erroneous decoding can result. Polar decoders are in serial nature leading to lower throughput compared to other schemes

In general, different FEC schemes can have significant differences in decoding performance, processing latency, and area requirements. Hence, an optimum FEC scheme is desired to well satisfy the requirements of the target application. To decide which FEC scheme is the best fit to the requirements of use-cases in WORTECS, the following performance metrics are taken into consideration.

1. Bit Error Rate performance (BER)
2. Throughput
3. Latency
4. HW Efficiency

A recent work published in [32] sets a comparison between the coding schemes in terms of the BER of different information block lengths (K), and code rates (R). The authors applied using Binary Phase Shift Keying (BPSK) modulation over the Additive White Gaussian Noise (AWGN) channel. LTE implementation for convolutional and turbo codes is chosen in this work. For LDPC, IEEE 802.16 codes are used, while using the Bhattacharya bounds algorithm to construct polar codes. The turbo decoder consists of two SISO decoders. Decoding of LDPC codes is performed with the Sum-Product (SP) Algorithm. The polar code decoding is handled by the standard successive cancellation (SC) decoding algorithm [33]. Some performance results can be shown in Appendix A.

Authors in [34] provided a comparison of hardware efficiency between polar, turbo and LDPC decoders in terms of area and time complexity of ASIC implementations. Here, the IEEE 802.11ad standard uses Quasi-Cyclic LDPC (QC-LDPC) codes with a block length of $K = 672$ and code rates $R = \{1/2, 5/8, 3/4, 13/16\}$. The authors simulated the performance of the IEEE 802.11ad LDPC code using a layered offset min-sum decoding algorithm. These metrics were plotted against each other on a double-logarithmic plot where the area and time complexity are on the vertical and horizontal axes, respectively. The hardware efficiency is defined as unit area per decoded bit and is measured in $\text{mm}^2/\text{bits/s}$. In addition, decoding throughput is the inverse of decoding time and denoted as T/P. metrics are also given in Appendix A.

Table 4 - Hardware efficiency of 3GPP LTE decoders

FEC Scheme	Metric			
	BER	Throughput	Latency	HW Efficiency
LDPC	Similar	High	Low	High
Turb1	Similar	High	Moderate	Moderate
Polar	Similar	High	High	Moderate

5.2 Description of digital baseband for OWC

The baseband design for the OWC transceivers needs to address two issues imposed by the optical front-end structure, i.e. the real valued and unipolar signal transmission due to intensity modulation (IM) used at the emitters. The standard OFDM, which is applied to the radio signals, is designed for complex and bipolar signals. Therefore, the standard OFDM design is modified to work with real-valued and unipolar signals. There are a number of variations of the OFDM to suit OWC, such as DC-biased optical OFDM (DCO-OFDM), asymmetrically clipped optical OFDM (ACO-OFDM), unipolar-OFDM, pulse-amplitude-modulated discrete-multitone (PAM-DMT), and Flip-OFDM. It is observed that in any OFDM scheme used for OWC transmission, a unipolar transformation process is required, e.g. asymmetrical clipping in ACO-OFDM or DC biasing in DCO-OFDM. The DCO-OFDM requires the least modifications compared to the standard OFDM, and hence we discuss this approach here in more details [35].

It is noticed that the required DC bias to satisfy non-negativity is equal to the maximum negative amplitude of the OFDM signal. Normally this can cause a clipping noise added to the signal, but if the DC bias is large enough, the clipping noise can be neglected. When a large number of subcarriers are used, the magnitude of the OFDM signal follows a Gaussian distribution with zero mean value. In this case, the amplitude of the OFDM signal would be less than 2σ with a probability of 97.8%, where σ is the standard deviation of the OFDM signal as a Gaussian distributed random variable. This, in practice, means the DC bias may be set to at least twice the amplitude of the signal. The value of the DC bias depends also to the modulation order, i.e. for larger constellations the DC bias must be larger to ensure unclipped signal [14]. The DC bias can be added to the signal at the optical front-end, however the disadvantage is low power efficiency of the scheme due to adding DC component.

The DCO-OFDM design shares main architecture and blocks with the standard OFDM architecture. In fact, main components and system parameters such as coding, scrambling and interleaving can be reused. However, since optical transceiver can process no phase information, and only works on real valued information, there need to have some modifications compared to the radio OFDM. This can be done by Hermitian symmetry transformation of the signal.

5.2.1 Hermitian symmetry OFDM

The architecture of the Hermitian symmetry OFDM transmitter is the same as the standard OFDM, except that it needs to deliver real-only data to the front-end. In addition, the transmitter needs to ensure all non-negative signals are delivered to the light emitter. The easiest way to achieve this is to add a DC bias to the bipolar OFDM signal, which can be done at the analog front-end. Meanwhile, to ensure the real-value signal the so-called Hermitian operation is used, in which half of the subcarriers are loaded with payload, and the other half are loaded with the complex conjugate values of the other half. It is observed this can be a simple buffering operation in practice. Figure 16 shows the architecture of the optical OFDM, which in contrast to the standard OFDM includes the Hermitian symmetry operation on the input stream to the IFFT block. In this case, to provide same data-rate as the radio OFDM system, the IFFT size is doubled. It is noted that a single DAC can be used however the sampling frequency would be twice compared to the one used for a standard OFDM transmitter. This is obviously a barrier in reaching a common architecture with the radio transmitter.

Likewise, at the receiver side, the standard OFDM can be used, with two differences. First, there is a buffering function as to get the complex symbols out of real-valued received signals. Second, there is no carrier frequency offset problem in optical front-end, as there no oscillator is used, and therefore no carrier frequency offset compensation is required. Hence the block diagram is pretty much the same as the one for the radio receivers as illustrated in Figure 17

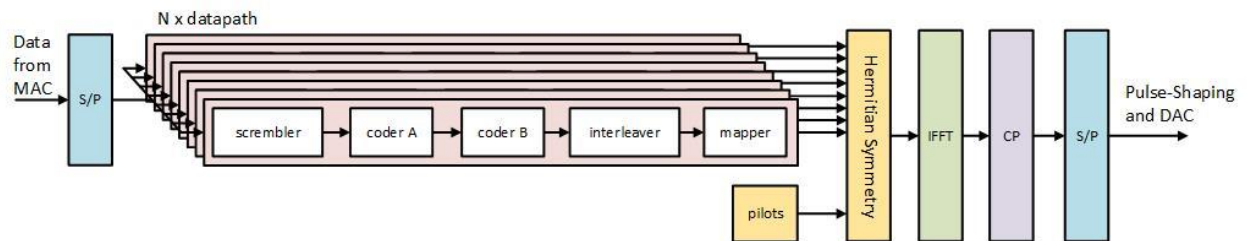


Figure 16 - Hermitian symmetry OFDM Tx architecture

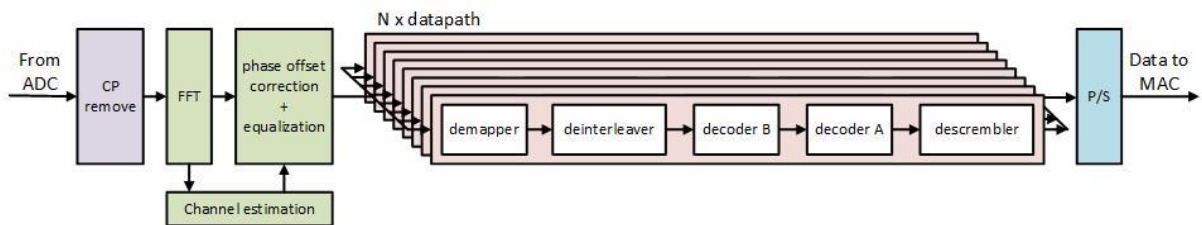


Figure 17 - Hermitian symmetry OFDM Rx architecture

5.2.2 Alternate approach: standard OFDM for OWC

As it is observed, in the Hermitian symmetry OFDM scheme, there are fundamental differences in the FFT/IFFT clock speeds, which is doubled for the optical transceivers compared to the one used in radio systems to obtain the same data-rate. On the other hand, a single DAC and ADC is used with a sampling rate twice compared to those for the radio system. The alternative approach would be to reuse the radio system architecture as much as possible. Hence it is proposed to upconvert the baseband signal to $B/2 + \epsilon$ where B is the bandwidth of the signal and ϵ is small compared to B . This is illustrated in Figure 18. As it is noted in the figure, not only the radio OFDM scheme can be reused, but also same DACs for the direct conversion radio transmitted can be used. The only difference would be the intermediate-frequency (IF) up conversion frequency equal to $B/2 + \epsilon$. The Rx can reuse ADCs and full standard OFDM scheme as well as it is illustrated in Figure 19.

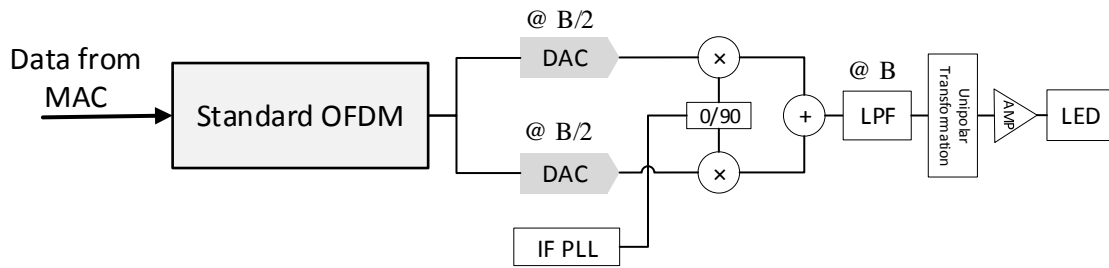


Figure 18 - Proposed Tx architecture for OWC

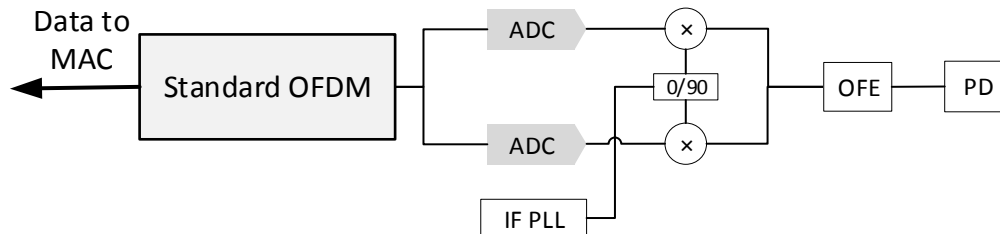


Figure 19 - Proposed Rx architecture for OWC

6 Common Radio and OWC architecture

6.1 Strong mutualisation

As discussed in 2.3, the radio and optical channel parameters are close enough to define a common OFDM system, even if it is not an optimal one for none of the two channels. Not only the data path function could be mutualized, but also the functions till the D/A and A/D converter. As described in 5.2.1, additional function to adapt relative complex number to natural real one are required but without impact on the system parameters. However, in order to keep a common sampling frequency and avoid the Hermitian sampling frequency improvement, light up and down conversion as described in 5.2.2 could be added in the optical analog front end.

6.2 Mutualisation example

Starting from the channel propagation characteristics (delay spread, time and frequency coherence) described in §2.3, we propose the following set of parameters for the base band design.

Table 5 - Mutualized OFDM system parameters example

Frame definition			
F_OL (GHz)	240,00	Doppler freq (m/s)	1,00
Fs (GHz)	2,16	tspread max (ns)	2,00
Ts (ns)	0,46	b_coh (MHz)	79,58
		t_coh (ms)	1,25
Efficiency (%)	93,00	Quasi const channel (SC nb)	18,86
Tofdm (ns)	26,57	Quasi const channel (Symb nb)	2452
Min FFT size suggested	57,39		
N_FFT	1024,00	Bandwidth Utilization (%)	80,00
CP size	77	User subc	819,00
CP (%)	7,51953125	Null subc	6
		Min Pilot Nb suggested	43,42
		Pilot Nb	50
CP length (ns)	35,65		
TsOFDM (ns)	474,07	Data Sc Nb	763,00
DeltaF (MHz)	2,11	Used Bandwidth (MHz)	1727,58

Frame parameters	
Channel bandwidth (MHz)	2160,00
FFT size	1024,00
Subcarrier Spacing (MHz)	2,11
FFT period (ns)	474,07
GI length (ns)	35,65
OFDM symbol length (ns)	509,72
Pilot nb	50,00
Null SubCarrier nb	6,00
Used Bandwidth	1727,58

We propose a framing that inserts time and frequency symbol pilots respecting the time and frequency coherence.

In an implementation point of view, the frequency interpolation of the channel using pilot distribution is quiet complex at such high sampling frequency. That is why we suggest to use a full preamble pilot as the first symbol of the frame.

Respecting the coherence time, and using an OFDM symbol length of 509ns, one full pilot should be inserted each 2452 symbols. An additional margin is used to prevent eventual high-speed movements, and also to track time and frequency synchronisation issues. By the way, a full pilot each 1000 OFDM symbols should be comfortable (as shown on the following figure, with X=1000).

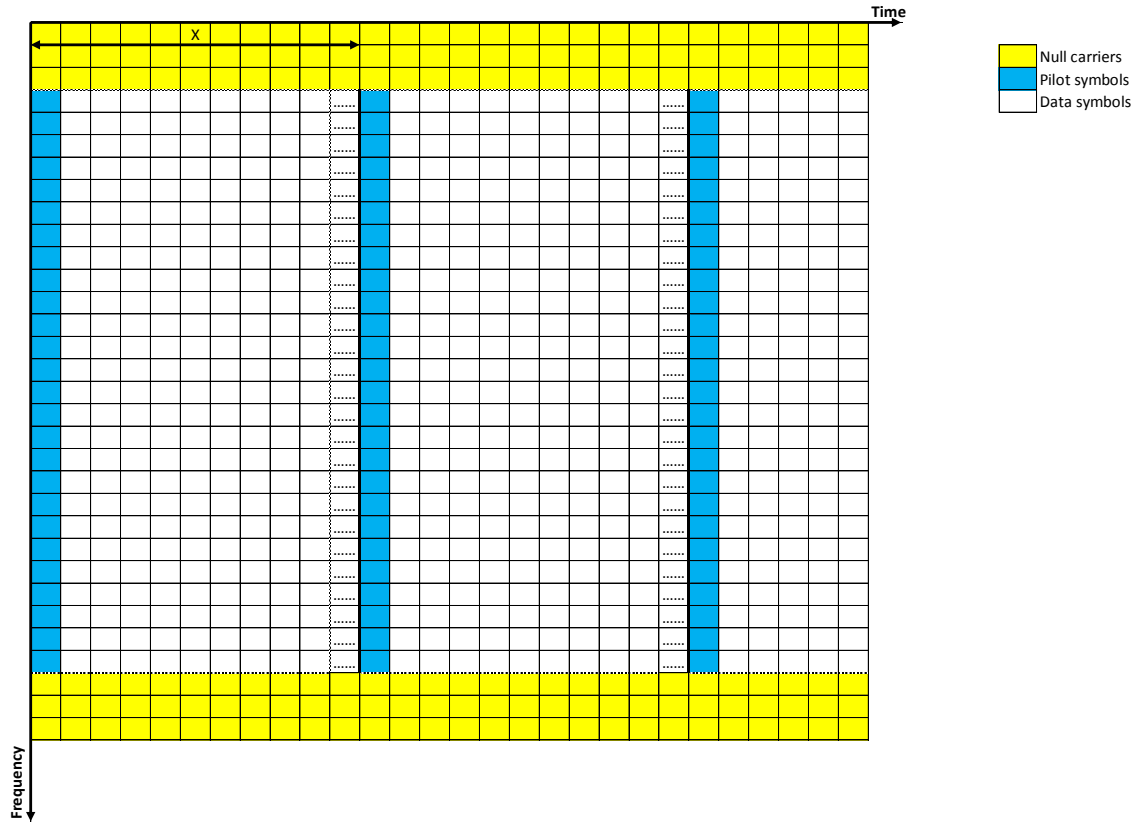


Figure 20: Proposed mutualized OFDM pilot position

6.3 Radio-optical common architecture

Based on the discussions in this deliverable, specifically the OWC transceiver architecture presented in section 5.2.2, we propose the architecture in Figure 21 and Figure 22. In the proposed scheme, the full OFDM based baseband design and DACs and ADCs are reused for the radio and optical transceivers. Moreover, both

approaches use in-phase and quadrature phase up conversions, but to different frequencies, i.e. to $f_{IF} = \frac{B}{2} + \varepsilon$

for the OWC, with B being the signal bandwidth and ε small value, and $f_{RF} = 240$ GHz for the radio system.

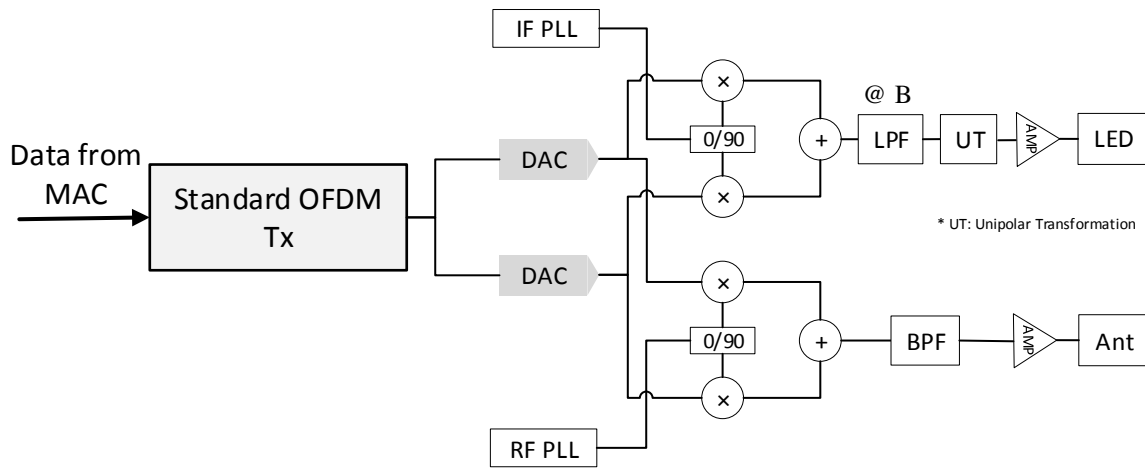


Figure 21 - Propose common Tx architecture: $f_{IF} = \frac{B}{2} + \varepsilon$, $f_{RF} = 240$ GHz

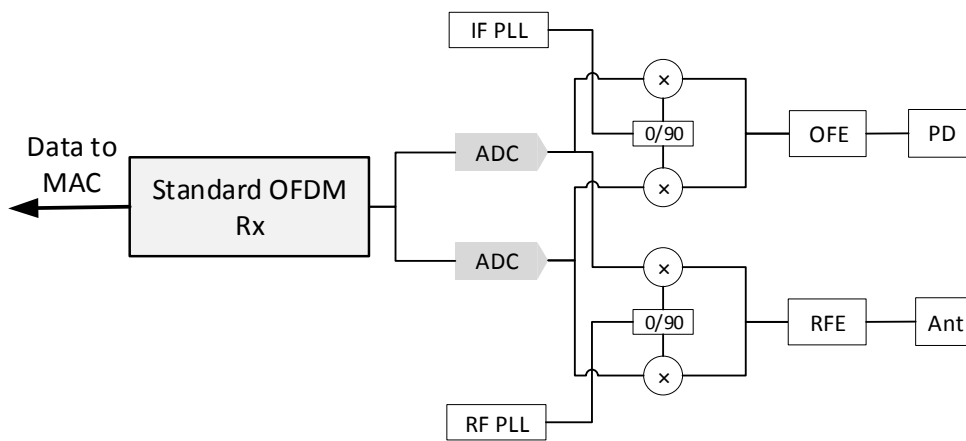


Figure 22 - Proposed common Rx architecture: $f_{IF} = \frac{B}{2} + \varepsilon$, $f_{RF} = 240$ GHz

7 Conclusion and perspectives

In this deliverable, we tried to answer the question of using as much as possible common components between a 240 GHz wireless radio and OWC systems.

Starting from their respective propagation channel characteristics, it is concluded that for the scenario under consideration, i.e. VR demo, the channel for both radio and OWC is LOS and frequency flat with very short delay spread. Hence the single carrier modulation seems the most appropriate transmission scheme at a first glance.

However, considering the very high operating frequencies of the transmissions the system is expected to experience various nonlinearities caused by HW components' impairments. So the overall equivalent channel becomes frequency selective and the use of multicarrier modulations, e.g. OFDM, are justified. Moreover, to take the decision about single- or multicarrier modulation, it is observed that due to its low complexity receiver implementation and spectrum efficiency OFDM is more favourable.

Then, detailed descriptions of the analog and digital designs for both radio and optical systems are given, taking into account the HW constraints in terms of component availability and cost. The whole design of the baseband architecture is specified targeting high data throughput, indicating the need of parallelizing some of the modules. The traditional OFDM designs for the OWC require Hermitian operation and some buffering to guarantee the transmission of real-value signals by the optical front-end. As this is a barrier in using maximum common

architecture due to its required IFFT size (double in optical system) the alternative approach of up converting the signal to half of the signal bandwidth (plus a small value) is proposed. By employing the proposed approach, the full baseband design, plus DAC and ADC components can be reused.

We keep in mind the interest to integrate the common architecture design in the same platform but it is not currently planned in the WP4 project roadmap.

8 References

- [1] Wortecs, "D3.1: Gbps wireless radio and Gbps wireless optical communication specifications and evaluations," Oct. 2018.
- [2] J. R. Barry, J. M. Kahn, W. J. Krause, E. A. Lee and D. Messerschmitt, "Simulation of multipath impulse response for indoor wireless optical channels," in *IEEE Journal on Selected Areas in Communications*, vol. 11, no. 3, pp. 367-379, April 1993.
- [3] F. Lopez-Hernandez, R. Perez-Jimenez and A. Santamaria, "Monte Carlo calculation of impulse response on diffuse IR wireless indoor channels," *Electronics Letter*, vol. 34, no. 12, pp. 1260-1262, 1998.
- [4] J. Lopez-Hernandez, R. Perez-Jimenez and A. Santamaria, "Modified Monte Carlo scheme for high-efficiency simulation of the impulse response on diffuse IR wireless indoor channels," in *Electronics Letters*, vol. 34, no. 19, pp. 1819-1820, 1998.
- [5] A. Behloul, P. Combeau and L. Aveneau, "MCMC Methods for Realistic Indoor Wireless Optical Channels Simulation," *IEEE Journal of Lightwave Technology*, vol. 35, no. 9, 2017.
- [6] D. O'Brien and al, "High-Speed Optical Wireless Demonstrators: Conclusions and Future Directions," *Journal of Lightwave Technology*, vol. 30, no. 13, pp. 2181-2187, 2012.
- [7] K. Miramirkhani, O. Narmanlioglu, M. Uysal and E. Panayirci, "A mobile Channel Model for VLC and Application to Adaptive System Design," *IEEE Communications Letters*, vol. 21, no. 5, 2017.
- [8] J. Carruthers, S. Carroll and P. Kannan, "Propagation Modeling for Indoor Optical Wireless Communications using fast Multireceiver Channel Estimation," [Online]. Available: <http://citeseerx.ist.psu.edu/viewdoc/download?doi=10.1.1.460.2678&rep=rep1&type=pdf>. [Accessed 10 01 2019].
- [9] WORTECS, "D2.2: WORTECS VR use-cases and requirements," 2018.
- [10] ITU, "ITU-R Radiocommunication sector of ITU, Attenuation by atmospheric gases, Recommendation ITU-R P.676-11, 2016."
- [11] A. Ekti, A. Boyaci, A. Alparslan, I. Ünal, S. Yarkan, A. Görçin, H. Arslan and M. Uysal, "Statistical modeling of propagation channels for Terahertz band," in *2017 IEEE Conference on Standards for Communications and Networking (CSCN)*, Helsinki, 2017.
- [12] S. Priebe, M. Jacod and Kürner T., "Angular and RMS delay spread modeling in view of THz indoor communication systems," *Radio Science*, vol. 49, no. 3, pp. 242-251, 2014.
- [13] "JPL's Wireless Communication Reference Website," [Online]. Available: <http://www.wirelesscommunication.nl/reference/chaptr03/cohbw/cohbw.htm>. [Accessed 25 01 2019].
- [14] D. Barros and et. al, "Comparison of Orthogonal Frequency-Division Multiplexing and Pulse-Amplitude Modulation in Indoor Optical Wireless Links," *IEEE Trans. Commun.*, vol. 60, 2012.
- [15] S. a. Z. B. a. Z. M. Samadi, "BANDWIDTH OPTIMIZATION TO ACHIEVE MINIMUM PHASE NOISE IN FREQUENCY SYNTHESIZERS," *IRANIAN JOURNAL OF SCIENCE AND TECHNOLOGY-TRANSACTIONS OF ELECTRICAL ENGINEERING*, vol. 38, pp. 21-32, 2014.
- [16] I. Dedic, "56Gs/s ADC : Enabling 100GbE," in *2010 Conference on Optical Fiber Communication (OFC/NFOEC), collocated National Fiber Optic Engineers Conference*, San Diego, CA, USA, 2010.
- [17] C. Kim, K. Kim, Y. H. Yun, Z. Ho, B. Lee and J. Seol, "QAM-FBMC: A New Multi-Carrier System for Post-OFDM Wireless Communications," in *IEEE Global Communications Conference (GLOBECOM)*, San Diego, CA, 2015.
- [18] X. Zhang, M. Jia, L. Chen, J. Ma and J. Qiu, "Networks, Filtered-OFDM - Enabler for Flexible Waveform in The 5th Generation Cellular," in *IEEE Globecom*, San Diego, CA, Dec. 2015.
- [19] F. Schaich, T. Wild and Y. Chen, "Waveform Contenders for 5G - Suitability for Short Packet and Low Latency Transmissions," in *IEEE 79th Vehicular Technology Conference (VTC Spring)*, Seoul, 2014.
- [20] Y. Liu and all, "Waveform Design for 5G Networks: Analysis and Comparison," *IEEE Access*, vol. 5, pp. 19282-19292, 2017.
- [21] B. Farhang-Boroujen and C. Yuen, "Cosine Modulated and Offset QAM Filter Bank Multicarrier Techniques: A Continuous-Time Prospect," *EURASIP Journal on Advances in Signal Processing*, vol. 2010, 2010.
- [22] X. Zhang, L. Chen, J. Qiu and J. Abdoli, "On the Waveform for 5G," *IEEE Communications Magazine*,

- vol. 54, pp. 74-80, 2016.
- [23] Y. Cai, Z. Qin, F. Cui, G. Y. Li and J. A. McCann, "Modulation and Multiple Access for 5G Networks," *IEEE Communications Surveys & Tutorials*, vol. 20, pp. 629-646, 2018.
- [24] M. S. K. K. M. E. M. Mohankumar, "Fpga Implementation of Mimo-Ofdm for Baseband Modem Parallel Architecture," *INTERNATIONAL JOURNAL OF ENGINEERING RESEARCH & TECHNOLOGY (IJERT)*, vol. 02, no. 03, 2013.
- [25] E. Satorius, "Parallel Modem Architectures for High-Data-Rate Space Modems," *Interplanetary Network Progress Report*, vol. 198, pp. 1-11, 2014.
- [26] B. T. a. S. S. a. M. Rupp, "BER comparison between Convolutional, Turbo, LDPC, and Polar codes," in *24th International Conference on Telecommunications (ICT)*, Limassol, Cyprus, 2017.
- [27] J. Z. a. R. Chen, "Achieving Transmit Diversity in OFDM-IM by Utilizing Multiple Signal Constellations," *IEEE Access*, vol. 5, pp. 8978 - 8988, 2017.
- [28] M. E. a. M. Petri, "60 GHz wireless broadband cable replacement for machine vision applications," in *International Symposium on Signals, Systems, and Electronics (ISSSE)*, Potsdam, Germany, 2012.
- [29] E. S. a. H. E.-G. a. D. McNeill, "Frequency offset estimation and correction in the IEEE 802.11a WLAN," in *IEEE 60th Vehicular Technology Conference, 2004. VTC2004-Fall. 2004*, Los Angeles, CA, USA, 2004.
- [30] T. Mohsnein, D. Truong and B. Baas, "Low-Complexity Message-Passing Algorithm for Reduced Routing Congestion in LDPC Decoders," in *IEEE Transactions on Circuits and Systems*, 2010.
- [31] A. Li, L. Xiang, T. Chen, R. Maunder, B. Al-Hashimi and L. Hanzo, "VLSI Implementation of Fully Parallel LTE Turbo Decoders," in *IEEE Access*, 2016.
- [32] B. Tahir, S. Schwarz and M. Rupp, "BER comparison between Convolutional, Turbo, LDPC, and Polar codes," in *2017 24th International Conference on Telecommunications (ICT)*, Limassol, 2017.
- [33] G. Berhault, C. Leroux, C. Jago and D. Dallet, "Partial sums generation architecture for successive," *Signal Processing Systems (SiPS)*, pp. 407-412, Oct. 2013.
- [34] A. Stimming, P. Giard and A. Burg, "Comparison of Polar Decoders with Existing Low-Density Parity-Check and Turbo Decoders," in *IEEE Wireless Communications and Networking Conference Workshops (WCNCW)*, San Francisco, CA, 2017.
- [35] S. Dissanayake and et. al, "Comparison of ACO-OFDM, DCO-OFDM and ADO-OFDM in IM/DD Systems," *Journal of Lightwave Technology*, vol. 31, no. 7, 2013.

9 Appendix A

Figure A.1 to Figure A.3 show the BER performance versus SNR for different FEC coding schemes of different information block lengths (K) adopting range of code rates (R). These results depict that turbo, LDPC and polar codes perform close to each other, which is the more true the larger the information block length (K).

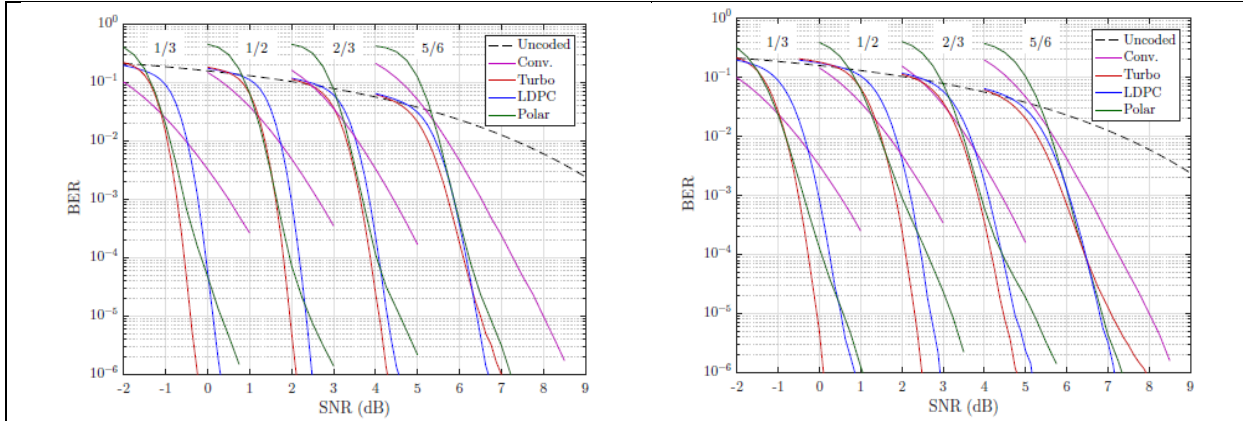


Figure A.1 - BER comparison for different code rates, $K= 512$ (For LDPC, $K= 516$ for $R= 1/2$, and $1/3$, and $K= 520$ for $R= 5/6$.)

Figure A.2 - BER comparison for different code rates, $K= 1024$ (For LDPC, $K= 1020$ for $R= 1/2$, $1/3$, and $5/6$.)

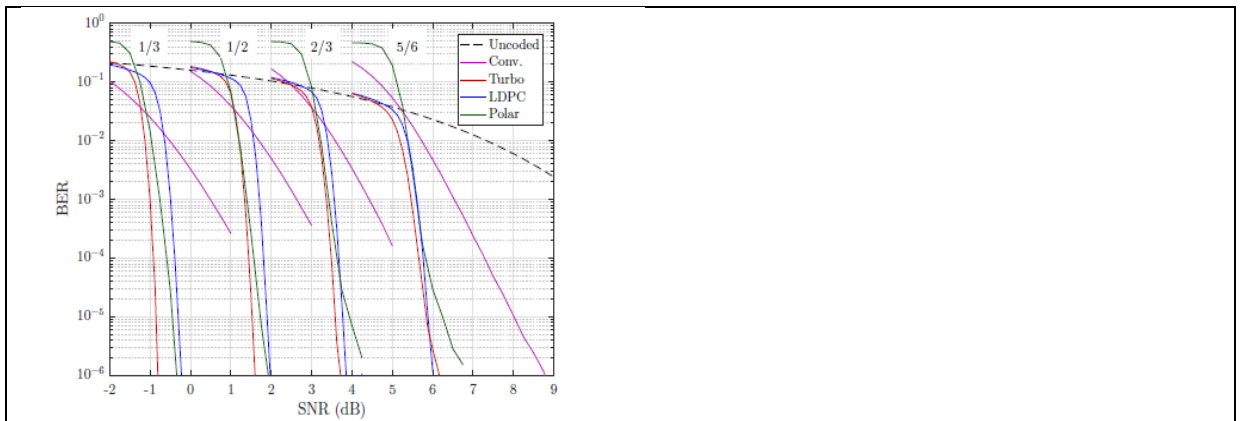
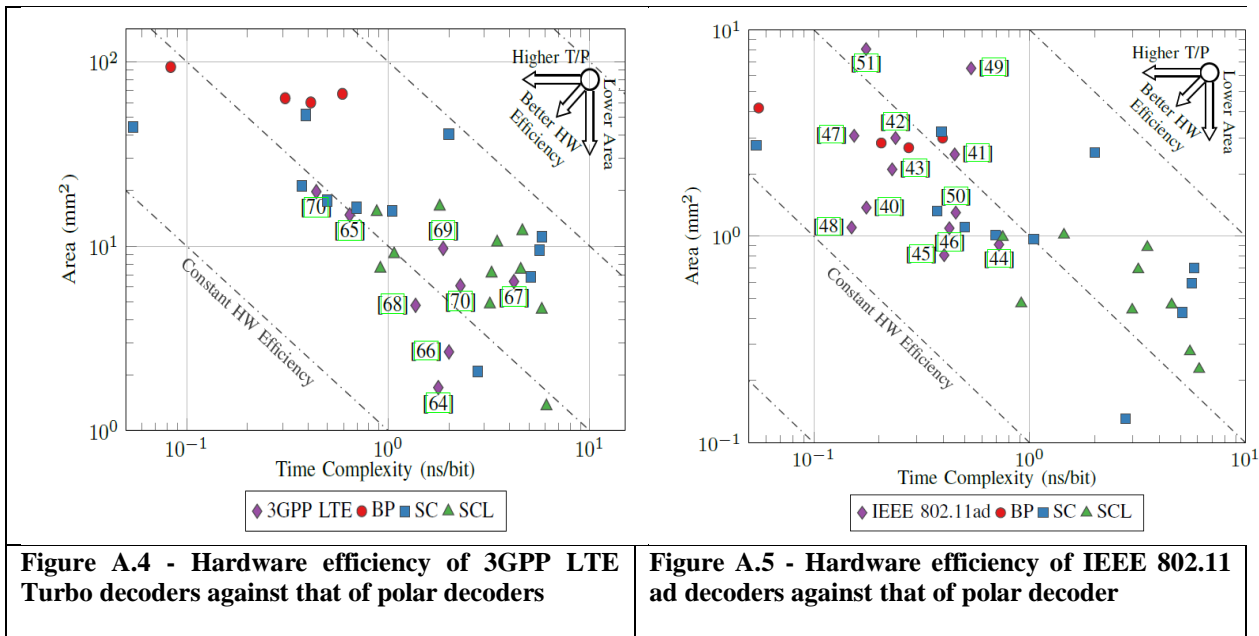


Figure A.3 - BER comparison for different code rates, $K= 8192$ (For LDPC, $K= 8196$ for $R= 1/2$, and $1/3$, and $K =8200$ for $R =5/6$.)



In Figure A.4, it is observed that, on average, the LTE Turbo decoders have similar hardware efficiency to the polar decoders. Moreover, it is noticed that polar BP decoders match the throughput of Turbo decoder at the cost of higher HW complexity. From Figure A.5, it can be seen that, on average, IEEE 802.11ad LDPC decoders have slightly higher hardware efficiency against polar BP decoders. While the hardware efficiency of polar SCL decoders is similar to LDPC decoders due to their lower area requirements, most SCL decoders have lower throughput. Based on the results shown, the table below summarizes the comparison of FEC schemes in terms of above-mentioned performance metrics.